MEYERSON, BERNARD STEELE

PREPARATION AND CHARACTERIZATION OF HYDROGENATED AMORPHOUS CARBON FILMS: ELECTRICAL AND OPTICAL PROPERTIES

City University of New York PH.D. 1981

Preparation and Characterization of Hydrogenated Amorphous Carbon Films: Electrical and Optical Properties

by

Bernard S. Meyerson

A dissertation submitted to the Graduate Faculty in Physics in partial fulfillment of the requirements for the degree of Doctor of Philosophy, The City University of New York.

1980

This manuscript has been read and accepted for the Graduate Faculty in Physics in satisfaction of the dissertation requirement for the degree Doctor of Philosophy.

12 Jan. 1981 — F. W. Smith
date — Chairman of Examining Committee

20 Jan. 1981 — [signature]
date — Executive Officer

[signature]

[signature]

[signature]

[signature]
Supervisory Committee

The City University of New York

Abstract

by Bernard S. Meyerson

Advisor: Professor Frederick W. Smith

There is considerable interest at present in the development of novel semiconducting materials, with the goal of establishing their potential usefulness in future device applications. Toward this end, a study has been undertaken to determine the properties of a material not widely regarded as interesting in terms of its properties as a semiconductor, ie. carbon in the form of thin amorphous films.

Semiconducting films of hydrogenated amorphous carbon(a-C:H) were prepared via the dc glow discharge of acetylene, at deposition temperatures T_d between 25 and 375C. The optical absorption(1.65 to 3.6eV) and electrical conductivity(25 to 350C) were measured. The electrical conductivity was not simply activated for samples with T_d<300C, and varied by over 10 orders of magnitude as a function of T_d. Optical energy gaps inferred from optical absorption data lay between 0.9 and 2.1eV, decreasing with increasing T_d. It has also been deduced from these measurements that these

a-C:H films will be graphitic in their electrical and optical properties for $T_d \geq 425C$.

Doped a-C:H films prepared via the incorporation of diborane or phosphine gas into the discharge have been studied. For a-C:H films deposited at T_d=250C, room temperature conductivity increased from 10^{-12} to $10^{-7} ohm^{-1}-cm^{-1}$ when either 1% phosphine or 10% diborane was added to the discharge gas. A shift of the Fermi level E_F of about 0.7eV was inferred from changes in the activation energy of conduction. The doping efficiency achieved here was comparable to that obtained in a-Si:H films produced in a like manner. Further verification of doping was obtained from measurements of the thermopower S performed on heavily doped samples (~1%dopant) prepared at T_d=325C. S was found to be positive for B doped samples, and negative for P doped samples. The magnitude of S, ~30uV/K, was indicative of a hopping transport mechanism, and such an interpretation is discussed in light of the result that S was found to be a nearly linearly increasing function of T ($300 < T < 550K$) for these samples.

As a result of the properties displayed by the a-C:H films studied here, one may arrive at the conclusion that this material holds promise for eventual use in the field of device technology.

Acknowledgements

I wish to express my gratitude to Prof. Fred Smith, who has been of immense help throughout the time this project was underway. He has been both advisor and friend, and has helped to make what might otherwise have been a grueling undertaking into one from which I derived a great deal of enjoyment. I have, in these last seven years of collaboration, been in the unusual situation of enjoying what I do, for which Fred was in large part responsible. I have considerable respect for his opinions as a physicist, and our many discussions in the course of this work have been invaluable in the assembly of this thesis.

I also offer thanks to the other members of my doctoral committee, who have, without exception, contributed to this work either through discussions, the procurment of needed experimental facilities, or both. In particular, I wish to thank Dr. Marc Brodsky, of IBM, for the extensive use given of the facilities available at the IBM T. J. Watson Research Center during the thermopower measurements. Also, thanks are due to Prof. Fred Pollack of Brooklyn College for the use of his reflectivity apparatus, and to Prof. Robert Callender of CCNY for the use of his spectrophotometer.

Table of Contents

page

List of Figures

INTRODUCTION

An area attracting a great deal of interest at present is the study of amorphous semiconducting thin films[1a]. Though the well characterized semiconducting materials such as single crystal silicon and germanium are the fundamental materials currently in use in the semiconductor industry, due to fabrication and processing expense they are not well suited to new applications such as the large scale arrays required for photovoltaics. Thus, there is now a great deal of work in progress researching alternative materials better suited to such applications. One class of promising alternative materials is that of amorphous semiconducting thin films. Amorphous semiconductors are themselves physically interesting in that they display the properties of a non-zero bandgap semiconductor, though they lack the long range order upon which the original calculations of band theory were predicated.

The most widely researched amorphous semiconductor at present is amorphous silicon(a-Si). Since 1975, when it was demonstrated[2] that glow discharge

prepared hydrogenated(hydrogen incorporated into the bulk) amorphous silicon(a-Si:H) could be doped, a great deal of work has been done toward more fully characterizing this material. As a consequence of this, a-Si:H is currently being employed in several test devices[1b], and further work is underway[1a]. Similar work is also under way on amorphous germanium[1a]. Unlike its two Group IV neighbors, amorphous carbon has not been widely researched regarding its properties as a semiconductor, and it is towards this aspect of amorphous carbon's behavior that my work is directed.

The two predominant naturally occurring forms of carbon are diamond, a large band gap semiconductor, and graphite, a zero band gap semi-metal. Amorphous carbon is a man-made material lacking the long range order found in these naturally occurring forms. Much of the prior work[3-5] on amorphous carbon films prepared via the glow discharge decomposition of organic vapors has been performed in relation to the fabrication of highly resistive dielectrics. Such films were referred to in the literature as organic polymer films, and were found to be hard, transparent, highly insulating ($\rho \sim 10^{12}\ \Omega$-cm) and of high dielectic strength. As films grown in such a manner have hydrogen incorporated in the discharge gas, and thus in the bulk of the sample, I will refer

to this material as hydrogenated amorphous carbon(a-C:H). Apart from the aforementioned studies of a-C:H as a dielectric, little systematic research has been done to investigate its properties as a potentially useful semiconductor[6]. Anderson[6] studied the semiconducting properties of a-C:H, but did not attempt doping, and thus a more detailed characterization. My thesis will present data in two sections, the first to include the data gathered during my work with undoped a-C:H, and the second segment to cover my experiments on doped a-C:H.

In the following section on theory, I will present the parameters generally utilized in characterizing amorphous semiconductors, as well as define each parameter according to current theory.

I) THEORY

In order to precisely define the basis of the various transport and optical parameters to be obtained further on, it is neccessary to first give an overview of the electron density of states one is referring to when discussing the region in and around the gap of an amorphous semiconductor.

The first question one must pose is that of the very existence of a gap in amorphous materials. As such a phenomenon relies upon the existence of non-overlapping valence and conduction bands, one must explain the presence of bands given the lack of long range order. Weaire and Thorpe[7,8,9a] proposed a Hamiltonian of the form

$$\mathcal{H} = \sum_{i,j\neq j'} V_1 \,|\phi_{ij}\rangle\langle\phi_{ij'}| + \sum_{i\neq i',j} V_2 \,|\phi_{ij}\rangle\langle\phi_{i'j}|$$

where ϕ_{ij} is the eigenstate of the jth sp^3 orbital at site i, V_1 a measure of the interaction between the orbitals at a given site, and V_2 represents the interaction of orbitals between sites, restricted to the case of nearest neighbor interaction. This Hamiltonian was applied to the case of a fully coordinated tetrahedrally-bonded solid, with j taking on values 1 through 4, and it was shown

that there must exist a region of zero electron state density(a "gap"), the dimensions of which are a function of the interaction potentials V_1 and V_2. A band gap of magnitude $E=2|V_2|-4|V_1|$ is predicted. This model, however, yields only the general features of band structure in tetrahedrally coordinated amorphous solids. It has been well established[9b,10,11] through various experimental procedures, such as ESR and DLTS(deep level transient spectroscopy), that there are significant electron state densities found within the "gap" of amorphous semiconductors.

Though the prior model does not predict or explain the existence of such states, an accepted view of their existence has been proposed by Mott and Davis[12a], in which these states are attributed to a series of narrow defect bands arising from the presence of unsatisfied(dangling) and strained bonds within the material. These "tail states", shown as the shaded region in Fig. 1.1a, lead to an imprecision in the definition of the term "gap" as it applies to amorphous materials. One solution is to redefine the term as a "mobility gap". The choice of this definition is made clear by an explanation of the phenomenon known as Anderson localization.

A calculation of localization found in Mott and Davis[12b] begins with the assumption of a periodic

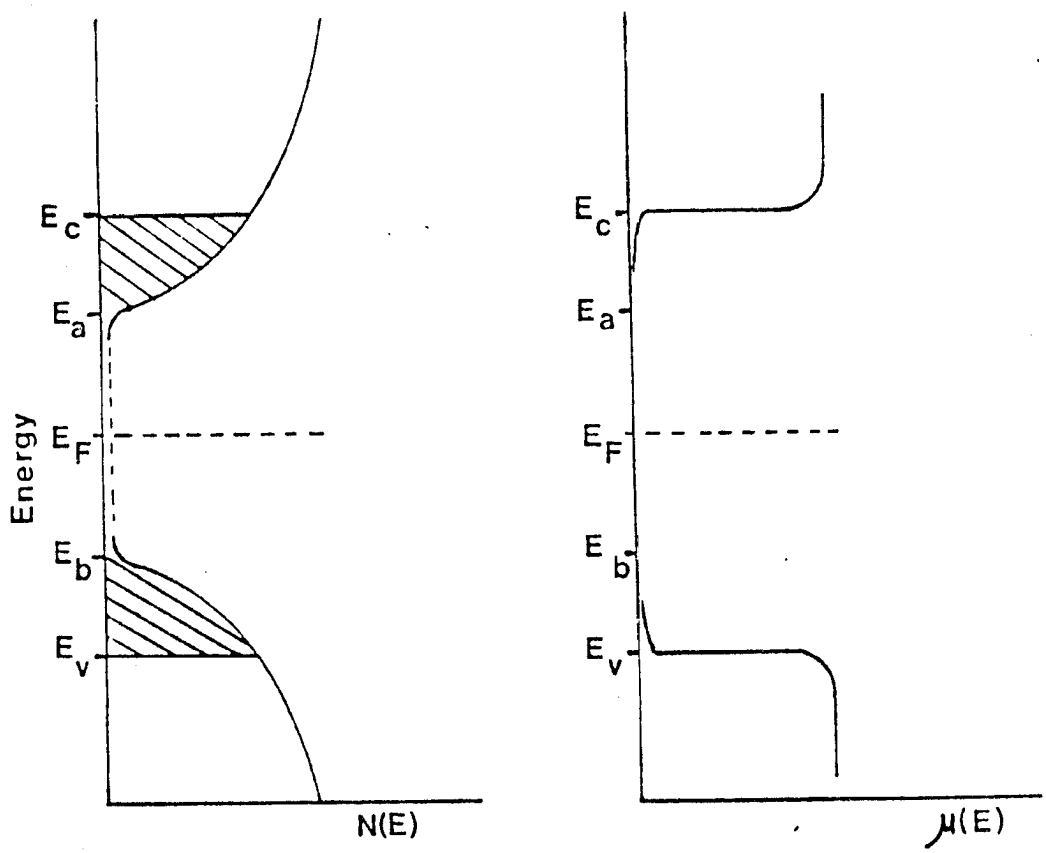

Fig. 1.1

(a) Schematic of the density of states in an amorphous semiconductor with localized states shown as the shaded regions. (b) Mobility gap, E_v to E_c, corresponding to accompanying density of states.

lattice with a random variation of potential well depth within the limits of $\pm V_o$. If one uses the simplest case of s-state atomic wave functions ϕ, one can define an overlap integral

$$I = \int \phi^*(\lambda - R_n) H \phi(\lambda - R_{n+1}) dV$$

R_n=coordinates of nth lattice site

which measures the electrostatic interaction, through H, of two neighboring electronic charge distributions as they are overlapped. For nearest neighbor interactions the above integral yields $I=I_0 \exp(-\alpha R)$, R being the intersite dimension, where the constant α is defined such that the expression $\exp(-\alpha r)$ defines the rate at which a wave function falls off away from its site. If one analyzes the probability at $T=0^oK$, that an electron will be found far from its site, it is found a critical condition exists such that for the case $\frac{V_o}{2zI} > c(z)$ (c a function of z with z being the coordination number), the probability that an electron would be found far from its site decreases as $\exp(-2\alpha r)$, effectively resulting in the localization of the wave function at that site. Thus, if this condition is satisfied, an electron's wave function assumes the form

$$\Psi = \sum_n A_n \phi(\lambda - R_n) \exp(-\alpha\lambda).$$

Conductivity data have been interpreted[12c,13] as the experimental validation of this concept via the

observation of a mobility edge, at which a sharp decrease in mobility occurs(Fig 1.1b). It should be noted that mobility edges may exist both above and below the gap. However, the one observed will depend upon the predominant mode of conduction, i.e. via electrons or holes. As a consequence, it is convenient to define a mobility gap, of magnitude E_c-E_v, which encompasses the region of localization. A review of a number of calculations of the coefficient c(z) in Anderson localization can be found in a review article by Thouless[14].

Given the existence of conduction and valence bands, as well as localized tail states within the gap, calculations can now be made regarding the physical manifestations of the band structure predicted for the amorphous materials to which this view of an amorphous semiconductor is applied. One should note the lack of detailed structure deep within the gap as shown in Fig. 1.1, this being a region whose detailed characteristics are not well understood through theory. Consequently, electronic structure deep within the gap has to be probed experimentally to complete the electron gap state density picture.

1) D.C. CONDUCTIVITY

The electronic transport mechanism at work within an amorphous semiconductor is thought to vary according to the ambient temperature under which this transport is taking place. The arguments I am about to make will apply to the case of transport by electrons, as in the case of an n-type semiconductor. The derivations may be quickly modified to the case of hole conduction with the substitution of $-E_b$ for E_a, $-E_v$ for E_c, and $-E_F$ for E_F. The three regimes of conduction thought to contribute to dc conduction are:

1) Conduction via extended states at or above the mobility edge located at E_c on the density of states diagram(Fig. I.1a).
2) Conduction via an activated form of nearest neighbor hopping in the localized tail states between E_a and E_c.
3) Conduction via variable range hopping in a narrow band of defect states centered about the Fermi energy.

a) EXTENDED STATE CONDUCTION

Starting with the Kubo-Greenwood formula[15,16] for the conductivity of a semiconductor, with $\mu(E)$ the mobility, $N(E)$ the density of states, and $f(E)$ the Fermi function, we get

$$\sigma(T) = -e\int N(E)\mu(E)kT\frac{\partial f(E)}{\partial E}dE \qquad (I.1)$$

One takes the derivative

$$\frac{\partial f(E)}{\partial E} = \frac{-1}{kT}\left[f(E)\left(1-f(E)\right)\right] \quad ; \quad f(E) = \left[1+\exp\left(\frac{E-E_F}{kT}\right)\right]^{-1}$$

yielding

$$\sigma = e\int_{E_c}^{\infty} N(E)\mu(E)f(E)\left[1-f(E)\right]dE \qquad (I.2)$$

Assuming a mobility edge at E_c, and taking $\mu(E)$ as $\mu(E_c)$ above the edge, we get

$$\sigma = e\,N(E_c)\mu(E_c)\int_{E_c}^{\infty} f(E)\left[1-f(E)\right]dE$$

if we assume $N(E)$ varies slowly about $N(E_c)$. As in this case we have conduction via extended states at or above E_c, and taking E_F to be roughly in the central region of the gap, $E-E_F \gg kT$, $\exp(E-E_F/kT) \gg 1$, so we may take $f(E) \cong \exp(-(E-E_F)/kT)$. Allowing for the fact that $f(E) \ll 1$, thus taking only terms to first order in $f(E)$, the integral becomes

$$\sigma = eN(E_c)\mu(E_c)kT\exp\left[-(E_c-E_F)/kT\right]$$

Utilizing the Einstein relation $\mu=eD/kT$, which cancels the temperature dependence of the prefactor, the resulting form of the extended state conductivity is

$$\sigma = \sigma_o \exp\left[-(E_c-E_F)/kT\right] \qquad \sigma_o = eN(E_c)eD$$

$$D(\text{diffusivity}) = (1/6)\nu a^2$$

If the band gap(E_c-E_v) decreases linearly with increasing T^{9g}, while E_F remains centered in the gap, then the <u>apparent</u> activation energy $(E_A=E_c-E_F)$ will also decrease linearly with T. To better define E_A, we take its value at $T=0^oK$, and allow for its apparent change in magnitude through the defining equation $E_c-E_F=E_A-\gamma T$. Using this definition, we get the expression

$$\sigma = \sigma_o \exp\left[-(E_A-\gamma T)/kT\right]$$

$$\sigma = \sigma_o' \exp\left[-E_A/kT\right] \qquad \text{(I.3)}$$

Thus, though E_c-E_F decreases linearly with increasing temperature, only the prefactor in the conductivity is altered. For conduction via extended states, the value of E_A obtained here from the slope of a plot of $\ln\sigma$ vs. $1/kT$ would be expected to set a maximum(as a function of T) for the activation energy to be observed in a given material. The value estimated by Mott[17] for σ_o in this case is in the range 10^1-$10^3\,\Omega^{-1}\text{-cm}^{-1}$.

b) CONDUCTION VIA NEAREST NEIGHBOR HOPPING

Starting from the same form of the Kubo-Greenwood formula(Eq I.2) we again derive the conductivity through the use of several simplifying assumptions. As conduction in the tail states takes place above E_a, and assuming $E_a - E_F \gg kT$, we can again express f(E) as $f(E) = \exp-(E-E_F/kT)$. In this case we may not remove the mobility μ from the integral, as we have thermally activated hopping through localized states, in which case μ can be expressed[9c] as

$$\mu = \frac{1}{6}\nu_{ph}\frac{eR^2}{kT}\exp[-W(E)/kT]$$

with ν_{ph} the maximum phonon frequency, R the interatomic dimension, and W the energy required to hop to the nearest site. A typical value of W can be estimated using the concept of this being a phonon assisted hopping process. Using $\nu_{ph} = 10^{13}$Hz, $E_{ph} = h\nu_{ph} = 0.06$eV This yields an estimate of W on the order of hundredths of an eV. The restriction of this phenomenon to nearest neighbors derives from the dropoff of Ψ as $\exp-(\alpha R)$, which for strongly localized tail states drives the wave function to near zero if one attempts to travel further than one site away.

Mobility, as calculated[9c] from the expression given above, has the value $\mu=10^{-2}cm^2V^{-1}s^{-1}$, a dropoff of approximately two orders of magnitude from its value in the case of conduction via extended states, and is thus indicative of the mobility edge spoken of earlier. Taking the case of a linear dropoff in the density of states from $N(E_c)$ to zero at E_a, one may use an expression of the form

$$N(E) = \frac{N(E_c)(E-E_a)}{(E_c-E_a)}$$

A slowly varying W(E) is assumed, thus W(E) becomes W_{av}. Using these assumptions and substituting in the expressions obtained, one finds

$$\sigma = \frac{e^2N(E_c)\nu_{ph}R^2}{(E_c-E_a)(6kT)}\int_{E_a}^{\infty}(E-E_a)\exp\left[\frac{-W_{av}}{kT}\right]f(E)[1-f(E)]dE$$

Keeping only terms first order in f(E), we get

$$\sigma = \sigma_1\frac{1}{kT}\int_{E_a}^{\infty}(E-E_a)\exp\left[-(E-E_F+W_{av})/KT\right]dE$$

Integrating by parts we get

$$\sigma = \frac{\sigma_1}{kT}\left[2k^2T^2\exp\left[-(E_a-E_F+W_{av})/KT\right]\right]$$

$$\sigma = \sigma_1'(T)\exp\left[-(E_a-E_F+W_{av})/KT\right] \qquad (I.4)$$

$$\sigma_1'(T) \equiv \frac{e^2N(E_c)\nu_{ph}R^2kT}{3(E_c-E_a)}$$

Thus, for the case of conduction in the localized tail states near the band edges, one expects to see a lower activation energy(E_A) for conduction than in the previous case as $E_a-E_F+W \lesssim E_c-E_F$, with $\sigma_1' < \sigma_o'$.

c) VARIABLE RANGE HOPPING

The third conduction process, and the one most likely to occur at low temperatures, is variable range hopping. As temperature decreases, the availability of high energy phonons to assist in hopping is diminished, thus increasing the chances that it may be statistically favorable that a hop occurs to the nearest site at an energy level within some small energy range U of the original, rather than to the nearest neighbor.

This model presumes the existence of strongly localized states in the region of the Fermi energy. Following the derivation by Mott[18], one begins with the assumption of a thermally activated hopping process in which only those states within an energy range kT of the Fermi energy are likely to participate, and, taking a slowly varying density of states about E_F, we get

$$\sigma = N(E_F)kT\,\Phi\left(\frac{e^2a^2\nu_{ph}}{kT}\right)\exp\left[-W/kT\right]$$

Φ measures the overlap between neighboring wave

functions, and in the context of hopping through localized states it contains a term $\exp(-2\alpha R)$, where R is a mean hopping distance. Taking $\Phi \cong \exp(-2\alpha R)$, one gets

$$\sigma = N(E_F) e^2 a^2 \nu_{ph} \exp[-2\alpha\lambda - W/kT]$$

If an electron jumps to a final state somewhere within a spherical volume of radius R about E_F, the number of states available in the energy range dE is

$$\frac{4\pi}{3} R^3 N(E_F) dE$$

Take the limiting case that there must be at least one available final state within the sphere,

$$\frac{4\pi}{3} R^3 N(E_F) dE = 1$$

and then define the jump energy W by

$$dE = \left[\frac{4\pi}{3} R^3 N(E_F)\right]^{-1} \equiv W$$

The jump frequency is given by

$$\nu_{jump} = \nu_{ph} \exp\left[-2\alpha\lambda - \left(\frac{4\pi}{3} R^3 N(E_F)\right)^{-1}/kT\right]$$

One can optimize ν_{jump} by setting the derivative of the above term with respect to R equal to zero, yielding

$$R = \left[\frac{9}{8\pi\alpha N(E_F) kT}\right]^{1/4} = \left(\frac{A}{T}\right)^{1/4}$$

This results in a jump frequency of the form

$$\nu_{jump} = \nu_{ph} \exp\left[\frac{-T_o}{T^{1/4}}\right] \; ; \quad T_o = 2.1 \left[\frac{\alpha^3}{kN(E_F)}\right]^{1/4}$$

Thus, the resulting expression for conduction via variable range hopping is of the form $\sigma = \sigma_2 \exp(-/T^{1/4})$.

$$\sigma_2 \equiv \frac{e^2 N(E_F)(.388)\nu_{ph}}{[\alpha N(E_F)kT]^{1/2}}$$

If all three regimes of conduction occur in an amorphous semiconductor, which is dependent upon the relative values of σ_0, σ_1, and σ_2, as well as the corresponding activation energies, a plot of $\ln\sigma$ vs. $1/kT$ could appear schematically as in Fig. 1.2 . As an example of the variations possible in this picture, consider the case where $\sigma_2 \gg \sigma_1$. Were this the case, it would be possible for the plot of region III to extend to region I, thus eliminating region II from the picture.

Apart from the Mott-Davis picture of conduction in amorphous solids, there is an alternative model that also predicts activated conduction, this being a model based upon small polaron hopping.

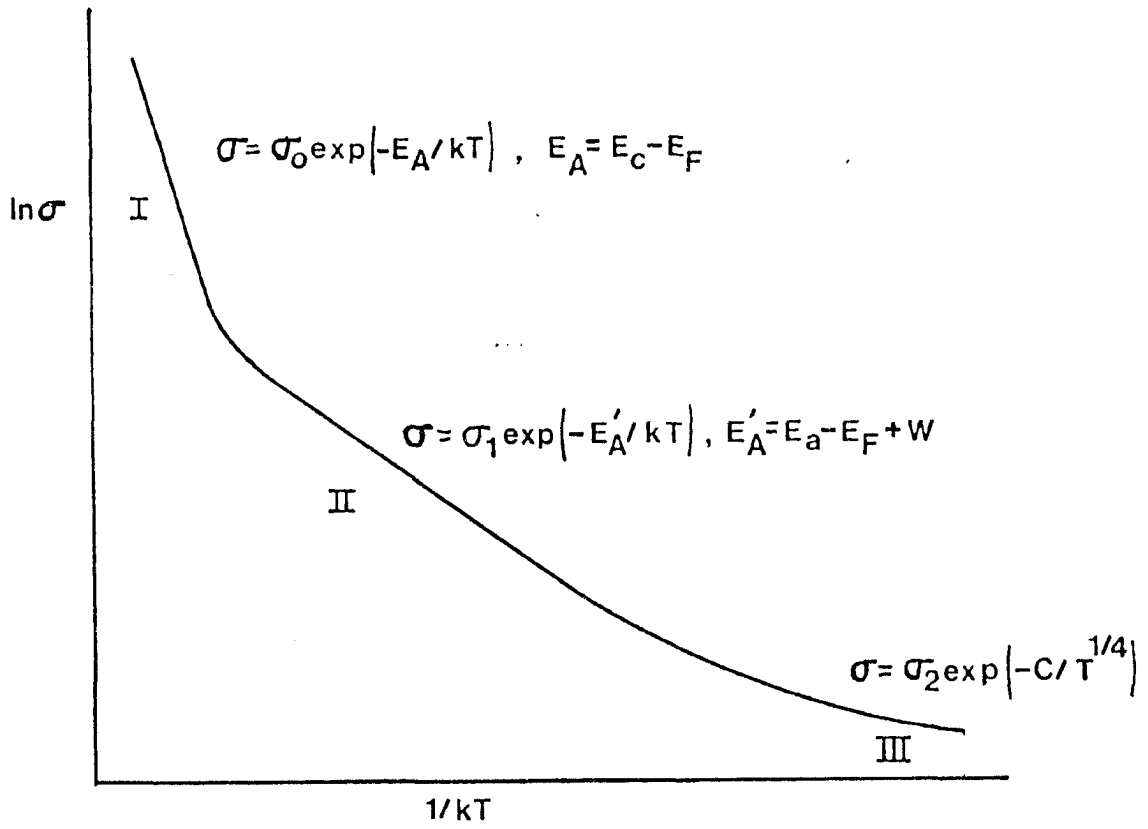

Fig. 1.2

Plot of $\ln \sigma$ vs. $1/kT$ for the case where all three regimes of conduction appear, namely conduction via extended states (I), nearest neighbor hopping (II), and variable range hopping (III).

d) SMALL POLARON HOPPING

Within the bulk of a solid, the presence of an unbound carrier inherently introduces a strain in the structure of the material surrounding it. If the distortion introduced causes a lowering of energy of the carrier, a bound state between the carrier and the strain may be formed, i.e. polaron formation. If this polaron travels through the material, one has the case of charge transport via small polaron hopping. There are two distinct cases to be considered for this mechanism.

The first regime is that of the adiabatic case of polaron hopping. In a material there are always small structural fluctuations taking place, thus making possible an event in which two neighboring sites are at the same energy as seen by the carrier. If a carrier is at one of these two sites and has sufficient energy to cross between sites, charge transport takes place. In the case where the carrier readily follows the lattice distortions, the process is referred to as adiabatic. The probability of charge transfer[9d], and thus the conductivity, varies as $\rho \cong C\exp(-W/kT)$, with the exponential representative of the chance that two sites are at the same energy level. "W" is defined as

the energy required to bring two neighboring sites to equal energies, thus allowing charge transfer to occur. In the adiabatic case, the probability of the carrier transferring when the energies of two neighboring sites coincide is taken to be unity.

When the carriers involved in transport react slowly to the instances where neighboring site energies coincide, it is the non-adiabatic case. As the carriers no longer follow the lattice distortions, the probability of transfer[9e,19] is taken as

$$P_2 = \frac{2\pi}{\hbar\omega_o}\left(\frac{\pi}{WkT}\right)^{1/2} J^2$$

where J is a measure of the overlap of neighboring wave functions, and w_o is a maximum phonon frequency. Then, again using the Einstein relation μ=eD/kT, where $D=a^2P_2$ is the diffusivity, a the intersite distance, and P_2 the jump probability, we get for the mobility in the non-adiabatic case the expression

$$\mu = C\left(\frac{1}{T}\right)^{3/2} \exp[-W/kT]$$

As a result, one should in this case observe an activated conductivity for $W \gg kT$, and a power law dependence for the case where $W \ll kT$.

2) POOLE-FRENKEL EFFECT

When working with amorphous semiconductors it is not unusual to observe a field-enhanced conductivity. This phenomenon is based upon the distortion of carrier traps within the material, which results in an exponentially increasing conductivity as a function of the field applied. A treatment of this is given by Connell et al.[20], where two conduction regimes, one a high field limit, the other a low field limit, are considered. The expressions for each case are given as

(Low Field Limit)

$$J_L = A(T)e\mu F \exp[(E_d-E_c)/mKT] \quad ; \quad \text{Trap Depth} \equiv E_d-E_c$$

(High Field Limit)

$$J_h = A(T)e\mu \frac{mKT}{\beta} F^{1/2} \exp\left[\frac{E_d-E_c}{mKT}\right] \exp\left[\frac{\beta F^{1/2}}{mKT}\right] \quad ; \quad \beta \equiv \frac{e^3}{\pi \epsilon \epsilon_o}$$

A(T) is a parameter describing the effective density of states and the degree of compensation, μ is the mobility, ϵ and ϵ_o are, respectively, the permittivity of the material in question and that of vacuum. The remaining parameters are m(allowed values of 1 to 2) which describes the statisitics used in determining state compensation within the material, and F, which is the electric field. Though several energy and temperature dependent parameters appear in these expressions, the number of assumptions needed as to

their behavior may be greatly reduced by working with the ratio

$$\frac{J_h}{J_L} = \frac{F_h^{1/2}}{(\beta/mkT)F_L} \exp[\beta F_h^{1/2}/mkT]$$

The value of ϵ may be obtained by solving the equation above for β using the values of J_h, F_h, J_L, and F_L obtained from high and low field conduction data, if such data fits well when plotted against the Poole-Frenkel expressions given earlier.

3) THERMOPOWER

Thermopower measurements are a valuable tool in the characterization and analysis of amorphous semiconductors. The thermopower S is defined such that $S=-\Delta V/\Delta T$. ΔV is the voltage difference that results from establishing a temperature differential T between the two points where V is being measured. In performing such experiments on amorphous semiconducting films, particularly those that are highly resistive, one encounters formidable experimental difficulties. However, the data obtained may yield valuable information on the conduction mechanism and the sign of the majority carrier. The sign of the majority carrier is a particularly valuable piece of information here in light of my experimentation on doped films of a-C:H.

A derivation of an expression for the thermopower in the case of an amorphous material was carried out by Cutler and Mott[21], starting from the integral form

$$S\sigma = -\frac{k}{e}\int_{E_c}^{\infty} \mu(E)\left(\frac{E-E_F}{kT}\right) f(E)[1-f(E)]N(E)dE$$

The assumptions utilized in evaluating this integral for the case of extended state conduction were

1) $E_c-E_F \gg kT$, so the Fermi function f(E) reverts to Boltzmann statistics, $f(E)\cong\exp(-(E-E_F)/kT)$
2) As $f(E)\ll 1$, only terms first order in f(E) are retained.
3) N(E) is slowly varying about E_c, allowing its removal from the integral as $N(E_c)$.
4) $\mu(E)=\mu(E_c)$, ie. μ varies slowly above E_c.

Carrying out the integration one gets the result

$$S = \frac{k}{e}\left(\frac{E_c-E_F}{kT}+1\right) \qquad (I.5)$$

Thus, at sufficiently high T to be in the regime of extended state conduction, one would expect to find the "activation energy" (E_c-E_F) observed in thermopower measurements identical to that obtained via conductivity measurements on the same material(see Eq. I.3 on pg.11).

It was suggested by Mott and Davis[12d] that in the case of nearest-neighbor hopping in the region about E_a, Eq. I.5 should be modified to read

$$S = \frac{k}{e}\left(\frac{E_a-E_F}{kT}+2\right) \qquad (I.6)$$

A point of interest here is that the "activation energy" in this expression for thermopower does not contain W, the hopping energy, thus making it possible to obtain W via comparison of thermopower data with conductivity data(see Eq. I.4 on pg 13). At this point it is neccessary to point out the limitations of this procedure.

In the temperature range where the conduction process in the material is in transition from nearest-neighbor hopping to extended state conduction, neither Eq.(5) nor (6) will be explicitly applicable. If this transition region is broad, it would not be surprising if a plot of S vs. 1/kT showed considerable curvature, making a precise determination of slope, and thus E_c-E_F or E_a-E_F , quite difficult. Lacking this information, W also may not be determined. Consequently, the data obtainable by this technique is limited in part by the sharpness of the transition between these two cases. Despite any questions arising from this difficulty, determination of the sign of the majority carrier is unaffected, and remains an important property to be determined.

A treatment of thermopower for the case of heavily doped amorphous semiconducting films was performed by Friedman[22], where an analysis of the properties of heavily doped n-type amorphous silicon was done. His

approach was to use experimental data on N(E)(gap state density), along with an assumed form for the mobility(u), in order to perform a series of numerical integrations of the Kubo-Greenwood formula. The advantage of such an approach is that it eliminated the need for many assumptions as to the behavior of N(E), and made no approximations as to the behavior of the Fermi function. His result verified that for the case of low temperature conduction, under the condition that

$$\frac{\partial}{\partial E} \ln(\mu N(E))\Big|_{E=E_F} \ll \frac{1}{kT}$$

the thermopower S behaves as predicted by the metallic formula,

$$S(T) = -\frac{\pi^2}{3}(kT)\frac{k}{e}\frac{\partial}{\partial E} \ln(\mu N(E))\Big|_{E=E_F} \qquad (I.7)$$

Based upon Friedman's result, an analysis of thermopower data obtained from heavily doped a-C:H samples is carried out in Section IV.2.

4) OPTICAL ABSORPTION

A great deal of information may be obtained by studying the optical absorption of an amorphous

semiconductor, yielding data on the composition, bonding, and band structure of the material[23]. Previous work[24-26] with amorphous carbon used I.R. absorption data to establish the presence of hydrogen within the material, as well as the manner in which it was bound. In a-Si:H, by observing IR absorption resonances and Raman scattering effects, determinations were made as to the relative numbers of SiH, SiH_2, and SiH_3 complexes present. The optical gap(E_{opt}) of amorphous carbon may be obtained using absorption studies made in the visible region of the spectrum, and this technique has been applied earlier by Anderson[6]. The majority of my own work has been done in the visible region of the spectrum, in order to determine E_{opt}(to be defined more precisely later), but I have also conducted I.R. absorption measurements to verify the presence of hydrogen in my samples, as well as to test for the presence of oxygen.

An expression for the optical absorption coefficient (E), that appears to fit well to several amorphous semiconductors, amorphous carbon included[6], was arrived at by Tauc[27], and Davis and Mott[28]. Davis and Mott start from the expression for ac conductivity,

$$\sigma(\omega) = \frac{2\pi e^2 \hbar^2 \Omega}{m^2 \omega} \int N_V(E) N_c(E+\hbar\omega) |D^2| dE$$

where Ω is the volume of the sample, and D is the matrix element of d/dx taken between the states involved in the transition. Taking $D=\pi(a/\Omega)^{1/2}$, "a" equal to the intersite dimension, the integral becomes

$$\sigma = \frac{2\pi^3 e^2 \hbar^3 a}{m^2} \int N_v(E) N_c(E+\hbar\omega) \frac{dE}{\hbar\omega}$$

Approximating the bands within the gap just above E_v or below E_c as having a linear density of states, ie. for the conduction band

$$N_c(E) = \frac{N(E_c)(E-E_a)}{(E_c-E_a)}$$

and assuming $\Delta E = E_c - E_a = E_b - E_v$, with $N(E_c) = N(E_v)$, the integral is

$$\sigma(\omega) = \frac{2\pi^3 e^2 \hbar^3 a}{m^2} 2 \int N(E_c)^2 \left[\frac{(E_b-E)(E+\hbar\omega-E_a)}{(\Delta E)^2}\right] \frac{dE}{\hbar\omega}$$

Evaluating this integral for the case that transitions are forbidden only if both the initial and final states are localized, and defining E_{opt} as (E_a-E_v), one gets

$$\sigma(\omega) = \sigma_o (\hbar\omega - E_{opt})^2 / (\hbar\omega |\Delta E|^2)$$

Using $\alpha = \frac{4\pi}{nc}\sigma(\omega)$, n equal to the refractive index, and σ_o the prefactor appearing in the expression for extended state conduction, one obtains

$$(\alpha E)^{1/2} = \alpha_o (E - E_{opt}) \; ; \; \alpha_o \equiv \left(\frac{\sigma_o n c}{4\pi |E_c - E_o|}\right) \; ; \qquad E = \hbar\omega \quad \text{(I.8)}$$

Thus, if we plot $(\alpha E)^{1/2}$ vs. E, and extrapolate the region of absorption above the optical edge(the energy above which strong absorption sets in) back to the E-axis where α equals zero(Fig. 1.3), we should find E_{opt}, the optical gap. It has also been shown[9j], if

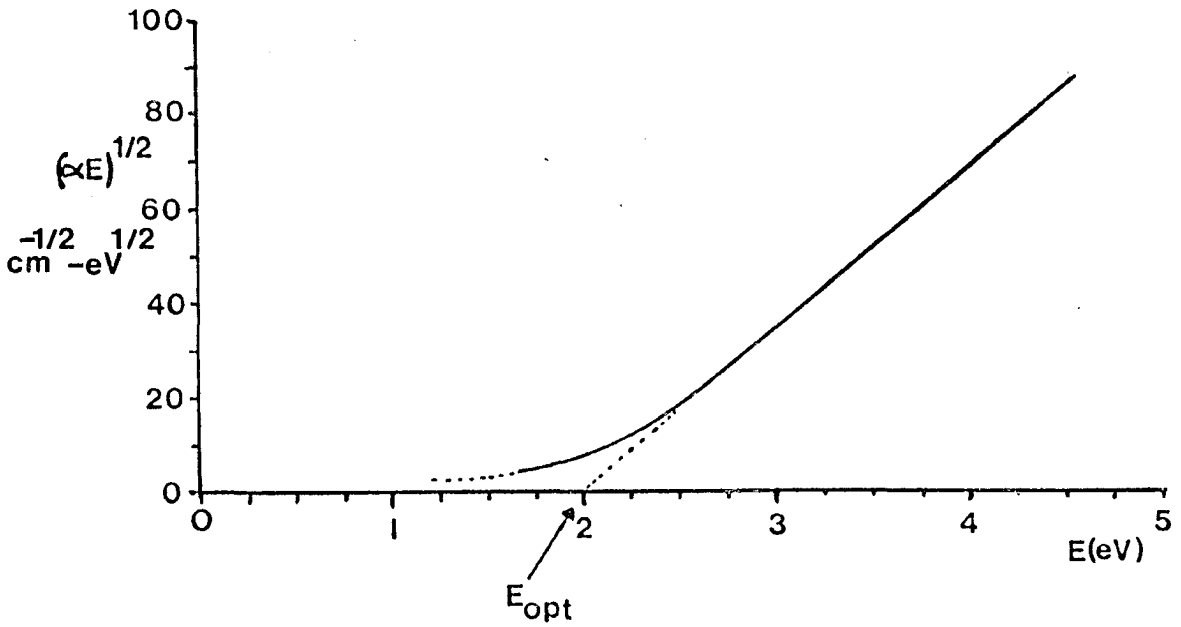

Fig. 1.3

A plot of $(\alpha E)^{1/2}$ vs. E for an amorphous semiconductor of optical gap(E_{opt})=2.0eV.

one starts from the assumption that the density of the tail states within the gap is parabolic, and all transitions involving localized states are discounted, one again gets the same functional form for the absorption as in Eq. (8), with E_{opt} now defined to be (E_c-E_v). If transitions are allowed in the case

where both the initial and final states are localized, one finds α behaves as

$$(\alpha E)^{1/3} \approx \text{const.}(E - E_{opt})$$

This form is regarded as unlikely as the interaction cross-section between two localized states is considerably less than that for localized to non-localized transitions, thus making it doubtful they should be included in such a calculation.

5) DOPING

As a semiconductor is substitutionally doped, its Fermi energy shifts within the energy gap. This phenomenon is a consequence of the creation of new states within the gap, either just above the valence band(acceptors) or just below the conduction band(donors). If shifts of E_A with doping reflect primarily shifts of E_F, then it is possible that through measurement of the observed shift in the Fermi energy, we may obtain a representation of the density of states found within the central region of the gap of a-C:H. A correspondence between $E_F = (E_{F_{initial}} - E_{F_{final}})$ and N(E) has been suggested by LeComber and Spear[9f], who

relate ΔE_F to N_D (density of donor states) by the expression

$$N_D = \int_{E_{F_o}}^{E_F} f(E)N(E)dE + \Delta N(E_c) \qquad (I.9)$$

(E_{F_o} is the Fermi level in the undoped material) $\Delta N(E_c)$, the number of donor electrons ionized to the conduction band, is taken as zero. It is pointed out[9f] that in an amorphous semiconductor, as there is a significant density of states present within the gap, it is likely that donor electrons, rather than being ionized into the conduction band, will cascade down to fill the gap states available just above the initial position of the Fermi level in the undoped material (E_{F_o}). As a result, the Fermi energy is shifted upwards in the gap towards E_c. A similar argument can be made for the case of p-type doping. In this case, acceptor states created just above E_v will be filled when electrons from higher occupied states drop down to fill these less energetic vacant states. Thus, the Fermi energy in this case is pulled towards the valence band.

If several simplifying assumptions are made, data on ΔE_F and N_D can yield a qualitative picture of the density of states N(E) within the central region of the gap. The assumptions are:

1) The Fermi function will be taken as a constant, equal to unity, below E_F.

2) The integral (Eq. 9) may be evaluated stepwise, ie. approximating the integration by summing a series of areas swept out by the Fermi energy as it moves through the gap.

3) The donor(acceptor) atoms are incorporated substitutionally at some constant fraction of the number of such atoms present in the discharge gas. This seems reasonable, as it has been found for a-Si:H[29] that approximately one out of two boron(B) atoms in a glow discharge with silane are incorporated in the resulting a-Si:H, and approximately one of every three incorporated B atoms in a-Si:H act as acceptors

Thus, for a-Si:H, a constant fraction($\sim$1/6) of the B dopant atoms in the discharge eventually function as acceptors. This strengthens the assumption that, to within a constant factor, a knowledge of N_D or N_A may be obtained through data on dopant concentration in the discharge.

Using the above assumptions, one gets the simple relation

$$N_p = N(E_{Fn} - E_{F_o})\Delta E_{Fn}$$

$$N(E_{Fn} - E_{F_o}) = N_D/\Delta E_{Fn} \qquad \Delta E_{Fn} \equiv E_{Fn} - E_{F,n-1}$$

which allows us to estimate the relative magnitude of the density of states at an energy removed by the amount $E_{F,doped} - E_{F_o}$ from the undoped Fermi energy. The

first two steps in such a process are shown schematically in Fig. 1.4 . Using the techniques above, I will analyze the midgap density of states in a-C:H, using data on changes in E_A, and thus E_F, as a function of doping.

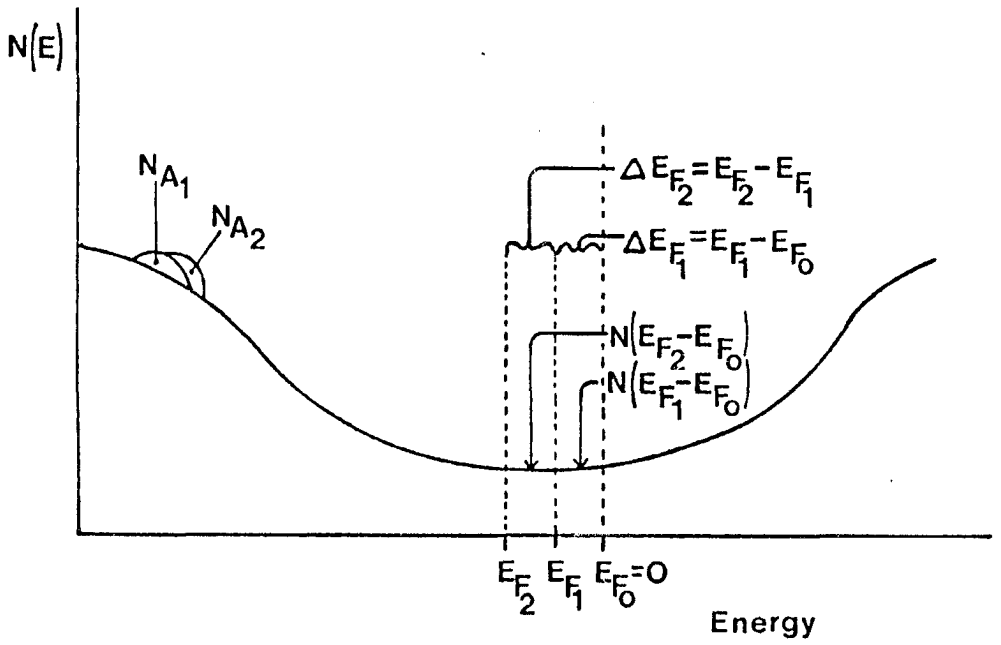

Fig 1.4

Technique for deriving N(E) from the shift of the Fermi energy accompanying doping, yielding $N(E_{F_1}-E_{F_o})=N_{A_1}/\Delta E_{F_1}$, and $N(E_{F_2}-E_{F_o})=N_{A_2}/\Delta E_{F_2}$,in the first two steps of this process.

II) EXPERIMENTAL PROCEDURES

1) EXPERIMENTAL APPARATUS

The samples studied here were prepared using a dc glow discharge apparatus (Fig. 2.1 and Fig 2.2). The configuration is that of a flow through device, ie. a continuous flow of reactant gas is passed through the region of discharge, with a typical flow rate of 0.8 sccm. It was found previously[3] that maintainence of such a flow reduced the chances of building up contaminants within the reactant gas during a discharge. The pumping of the discharge chamber is accomplished by two systems. For preliminary pumpdowns, a Veeco VS-9 pumping station is used, its two inch air cooled diffusion pump achieving final pressures on the order of 10^{-7}Torr. Pumping during the discharge, and thus involving reactive gases, is accomplished via a separate neutralization and disposal system (Fig. 2.3). Use of such a system is neccessitated by the presence of corrosive and toxic dopant gases during the doping experiments, namely B_2H_6 (diborane) and PH_3 (phosphine). Neutralization is accomplished via both pyrolysis at 750C in a Mullite furnace tube, as well as by bubbling the gas through a neutralizing solution.

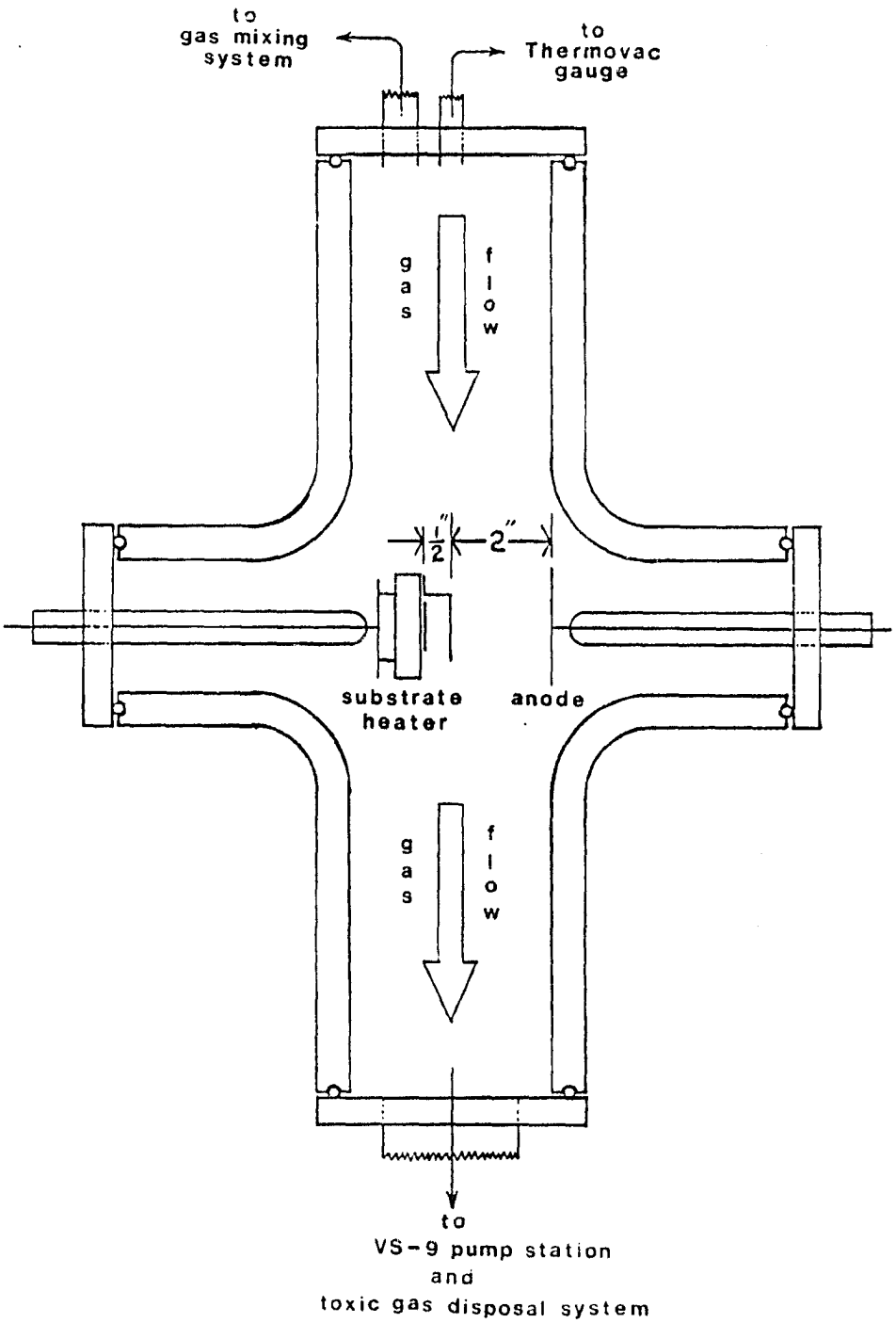

Fig. 2.1

The dc glow discharge apparatus used in the preparation of samples used in this study.

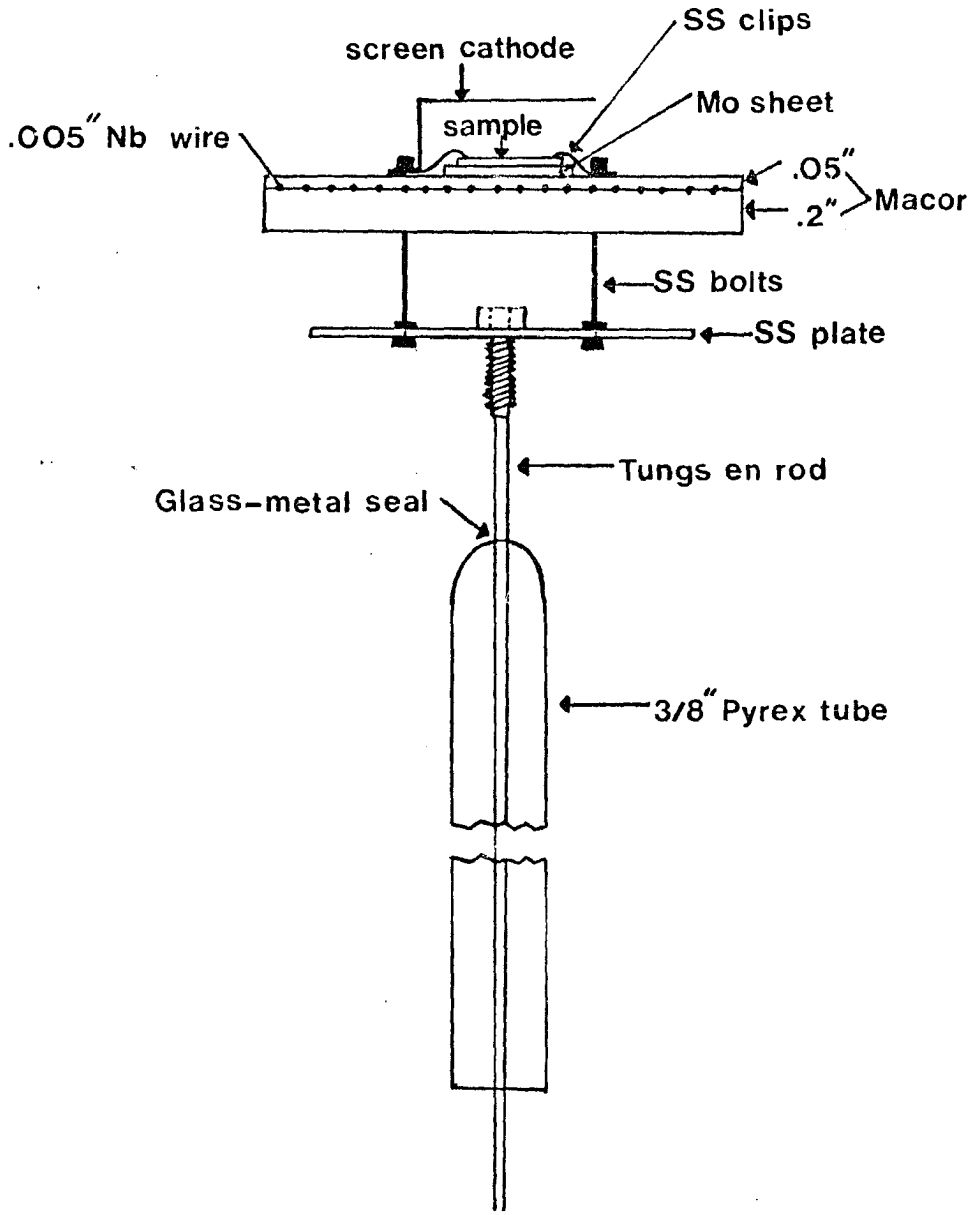

Fig 2.2

Detailed diagram of the substrate heater assembly used in sample preparation

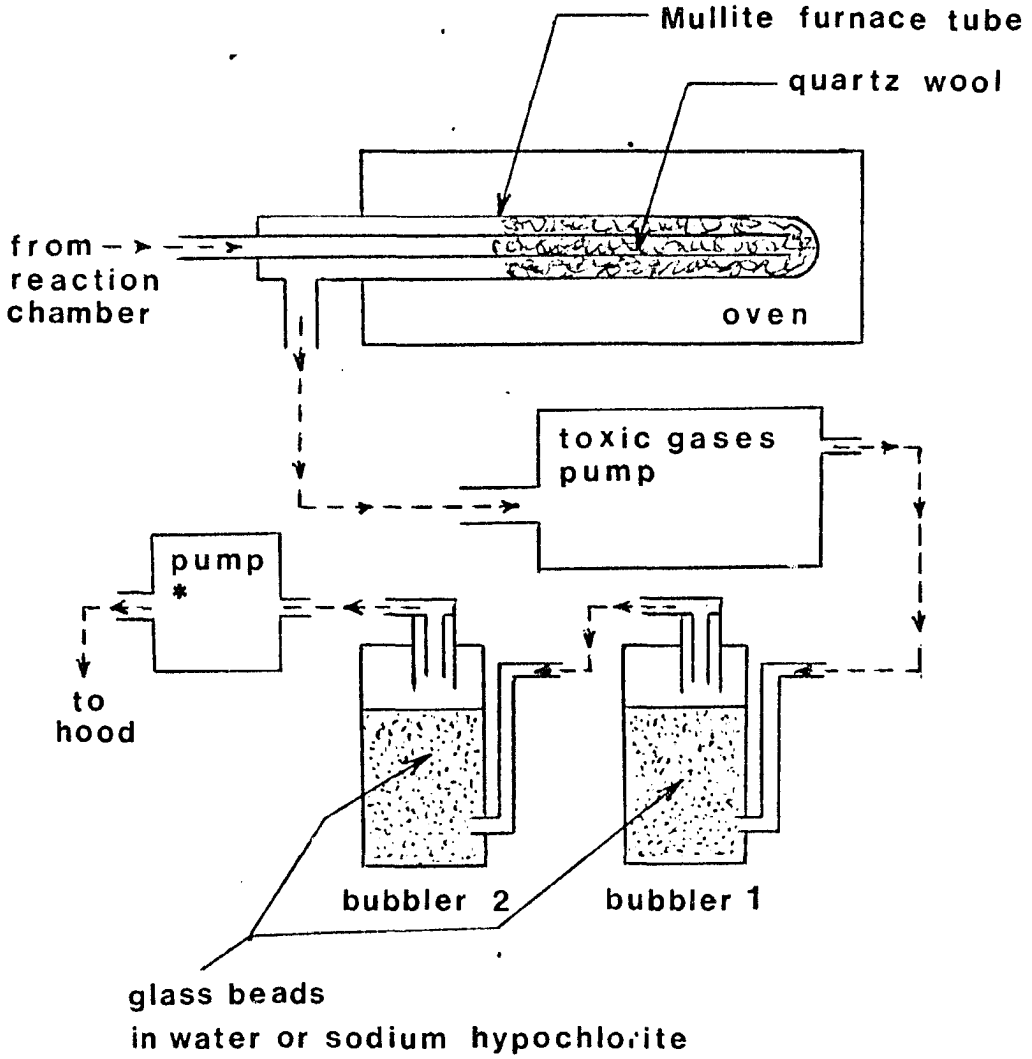

Fig 2.3

Gas neutralization and disposal system

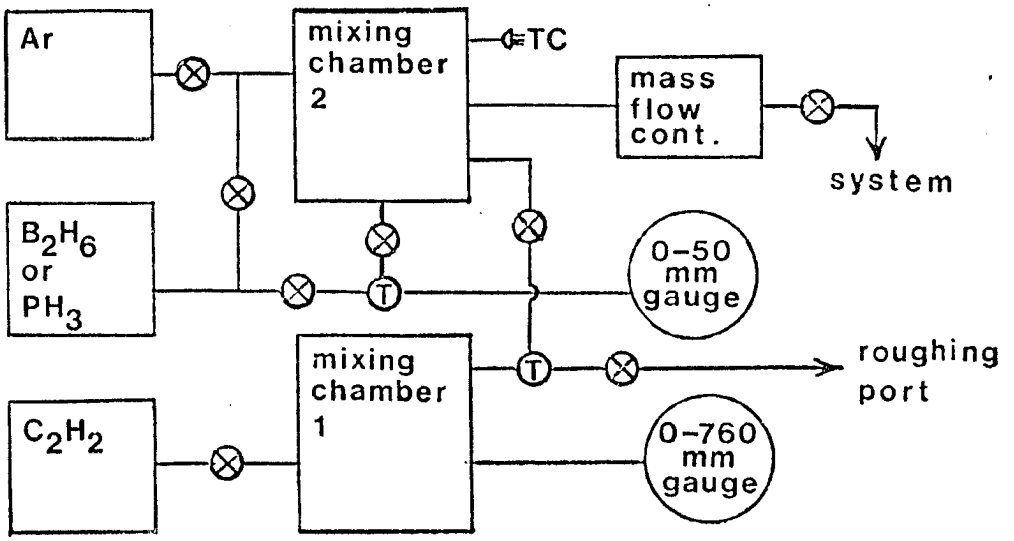

Fig 2.4

Gas mixing and flow control system

For the oven tube and the bubblers, quartz wool and glass beads, respectively, are placed in the path of the gas, thereby shortening the mean free path of the molecules, and increasing the probability of neutralization. Though pyrolysis should completely decompose the gas, the bubbling process serves as a backup in the event of oven failure or power loss, as the bubblers would continue to function in either case. As diborane hydrolyzes in water at room temperature, H_2O serves as the neutralizing solution. When the dopant gas is phosphine, sodium hypochlorite (household laundry bleach) is used. The

pump used to remove the waste gases and thus maintain a constant pressure during the discharge is a corrosion resistant Leybold Heraeus Model D8A rotary vane pump. Data on the safe handling, disposal of, and emergency procedures for the gases above is available in two texts from Matheson Gas[30,31](given the high toxicity of the dopant gases, the presence of these references or their equivalent is highly advisable).

The sample substrate(typically 18mm x 18mm x .25mm) is mounted on a substrate heater(Fig. 2.2) constructed of Macor, a Dow Corning ceramic, with the heat supplied by the ohmic heating of 0.005" diameter Niobium wire encased in the Macor. Macor is well suited to such applications as it is a non-porous insulator that is stable up to 1000C, sufficient for this application. The substrate sits above a sixteenth inch plate of molybdenum, utilized to insure a uniform temperature distribution across the sample. Temperatures are measured with a chromel-alumel thermocouple clamped to the front surface of the sample. An unheated stainless steel screen cathode is mounted approximately one centimeter above the face of the sample, its purpose to increase deposition rates as well as to localize the discharge. All metal components of the system, other than the clips holding the sample and the screen cathode, are electrically floated. This serves to

furthur localize the discharge to the face of the sample, thus reducing the chances of contamination due to the discharge ejecting material or adsorbed gas off the walls of the chamber. A stainless steel(SS) plate covered by a SS screen is utilized as a cold anode, the screen being added to increase the surface area of the plate, thus reducing the likelihood of charge buildup and arcing during discharges at relatively high currents. The power source used to maintain the discharge is a Hipotronics Model 803-330 (3000V, 400ma) dc supply, typical operating parameters being 350 volts at 3 ma. The substrate heater was powered by a Kepco dc Power Supply(0-30V, 2A), typically operated at 12-24 volts supplying 1-2 amperes.

A late addition to the system was a heated cathode screen, which could be baked at temperatures above 600C, the importance of which will be explained later. The above screen was also fabricated of Macor and niobium wire, and was powered by the above mentioned Kepco power supply.

Gas mixing and flow control were provided by a gas handling system, a schematic of which appears in Fig. 2.4. The system can provide three gases at a time, argon(99.9%), commercial grade acetylene (C_2H_2-99.6%) dissolved in acetone, and either diborane(1%B_2H_6-99%Ar) or phosphine (1%PH_3-99%Ar), depending upon the doping experiments to be conducted. All system components are

constructed of materials rated for corrosive service. The system can supply dopant gas/acetylene mixtures in ratios varying from 10^{-6}:1 to 10^{-1}:1, with an accuracy of better than 1% for ratios above 10^{-5}:1, and within 10% below that level. Flow control for the system is provided by a Union Carbide Mass Flow Controller, model FC-260(0.1-10sccm), calibrated for acetylene. Provisions have also been made for the purging of the system with an inert gas(Ar) before and after use, as reactive and corrosive compounds can form if the dopant gases are introduced into the system in the presence of moisture, or if the reverse occurs.

2) SUBSTRATE PREPARATION

Substrates utilized in these experiments varied according to the analysis technique to be applied. For conductivity studies on samples prepared at temperatures below 350C, Fisher microscope cover slips(18 x 18mm., Thickness #1) were used. The slides were cleaned in an ultrasonic cleaner for approximately one minute using a solution of water and transene ultrasonic detergent(TUD), then rinsed in triple distilled, deionized water, after which they were blown dry with nitrogen gas. The slides were then placed in a NRC 3117 vacuum system equipped with an electron beam

evaporation system(Fig. 2.5). A molybdenum source was placed in the e-gun hearth, and a 1000A layer of molybdenum was evaporated onto the slides. The thickness of the layer was monitored during depostion by an Inficon deposition rate monitor. To insure good adhesion of these films, as well as freedom from pinholes, I found it to be crucial that the hearth of the e-gun be free of all deposits, as flakes of material ejected off the hearth during deposition ruined the films resulting from that particular run. Also, any trace of liquid allowed to dry on the surface of the slides precluded adhesion of the films to that area. An additional technique that aided in the fabrication of high quality substrates was the melting and outgassing of the molybdenum source material in an arc furnace prior to its use as the e-gun target. Trapped gas within the molybdenum source had made stable evaporations difficult, as gas bursts occurred when the gas blew out of the molten metal, spraying the system with drops of white hot molybdenum, thus posing a considerable safety hazard. By outgassing the molybdenum in the furnace, this problem was virtually eliminated.

When samples were to be prepared at temperatures equal to or above 350^{o}C, changes in substrate preparation were neccessary to allow for the fact that samples prepared in this temperature range showed

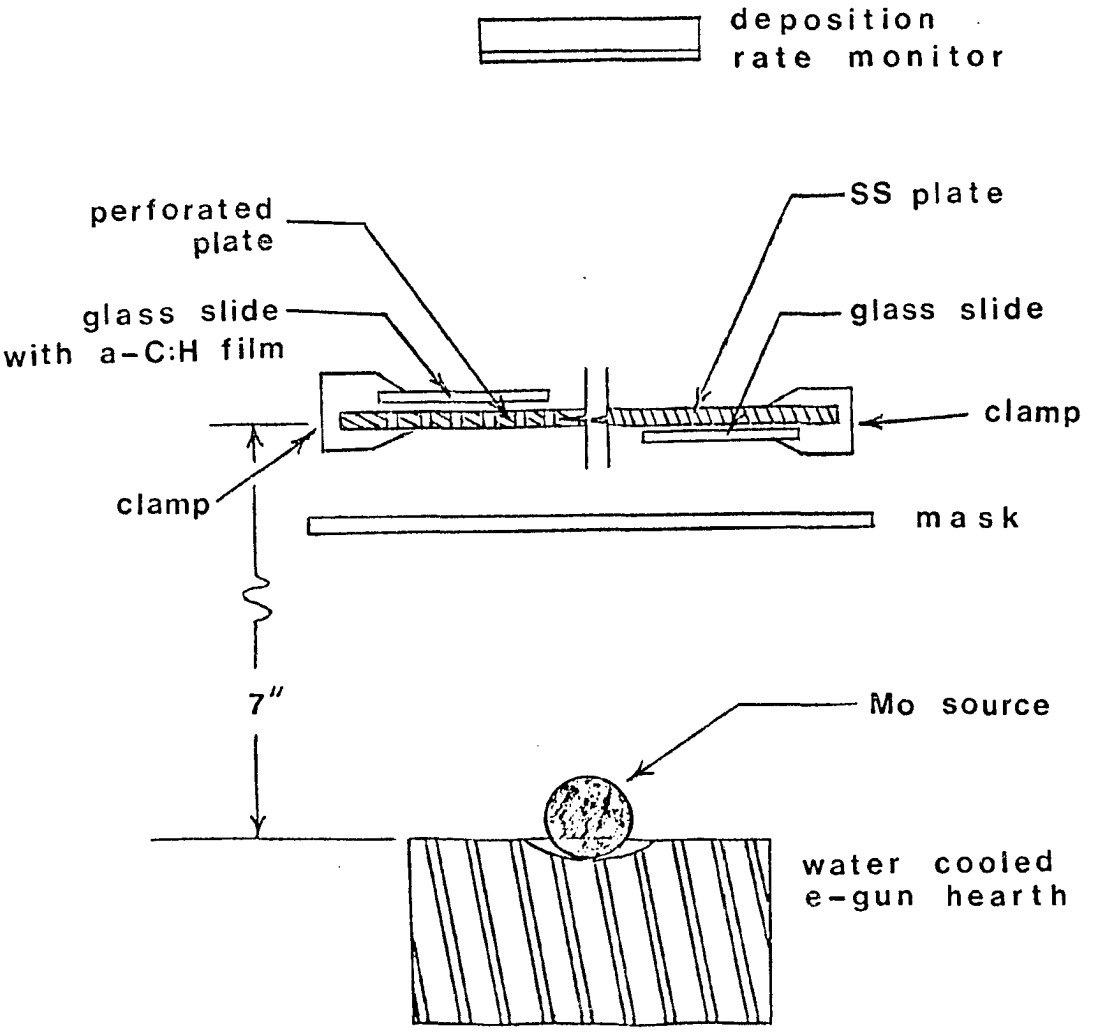

Fig. 2.5

Setup for molybdenum deposition. The left side of the diagram shows the sample mounted for the deposition of the Mo dots. The right side of the diagram shows the setup for substrate preparation, ie. deposition of the initial Mo film.

resistances as low as 100 ohms(measured at 250C when using the sandwich geometry described in the following section). As the resistance across the molybdenum film on a typical substrate was roughly 30 ohms, accurate measurement of sample resistance was impaired by the substantial contribution of the substrate. This difficulty was circumvented by the deposition of a thick layer of aluminum on the slides first, followed by the deposition of a 1000A molybdenum layer to serve as a diffusion barrier(to prevent aluminum from diffusing into the a-C:H during the discharge). This lowered the resistance across the substrate surface to below 1 ohm, and facilitated accurate conductivity measurements.

Substrates used in optical absorption studies, either in the visible or infrared region of the spectrum, were cleaned in the same manner as before, but had no metal layer deposited on them. For the determination of E_{opt}, data was taken in the visible range, allowing use of the glass slides mentioned earlier. For infrared absorption, substrates of either silicon or sapphire were used, their dimensions similar to those of the glass slides.

3) SAMPLE PREPARATION

Once the substrates were prepared as described in the preceding section, they were mounted on the face of the substrate heater(Fig. 2.2), and the heater assembly was then mounted in the deposition system(Fig. 2.1). The entire system, including the gas mixing and flow control system, was rough-pumped by the gas disposal system to a pressure below 0.1 Torr. The system was then brought up to atmospheric pressure by back-filling it with dry argon gas, and then pumped again, with this flushing procedure being repeated three times. After the final rough pumpdown, the VS-9 pump system was turned on, and the system was pumped overnight to a final pressure of about 2.0×10^{-7} Torr. This final pressure made a good qualitative indicator of how leaktight the system was, as final pressure was significantly increased by very small leaks at any seal. On the first run of a series, or after the system had been opened to the atmosphere, the gas mixing system would be baked out, and another overnight pumpdown would take place to insure removal of the gases evolved. When this was not the case, the mixing system was isolated from the discharge chamber, and gas mixing took place.

Several options are available as to the method used in mixing the gases, and they vary according to the ratio of gases required. The simplest case is when undoped a-C:H is fabricated, where the entire mixing system was filled to a pressure of 400 Torr with C_2H_2, after which the acetylene tank was sealed off. The gas is then fed to the system through the mass flow controller at the desired rate. The choice of 400 Torr is made mandatory by the flow controller, which must have a pressure differential of at least one half atmosphere across it in order to function properly.

When doping was to be performed, at concentrations of dopant to C_2H_2 below a ratio of 10^{-4}:1, mixing chamber 1(MC1) and mixing chamber 2(MC2) were isolated from each other, after which MC1 was brought to a pressure of 800 Torr C_2H_2. At this time, MC2, and the 0-50 Torr gauge, were brought to the desired pressure of the 1%dopant-99%Ar mixture, such that when the two sections of the system were combined, the desired ratio would result. When filling MC2 with dopant, the dopant tank valve was first opened and closed, pressurizing the regulator. The dopant gas was then drawn from the high pressure side of the regulator with the tank valve closed. There was sufficient gas in the high pressure side of the regulator to achieve any ratio desired. This procedure reduced the risk of back-diffusion of contaminants into the dopant gas

tank, as well as limiting any possible leakage of dopant gas from the system to the amount of gas already in the regulator. It was easily calculated that this amount of gas would not pose a significant hazard if dispersed in the lab. Using knowledge of the relative volumes of the system occupied by each gas ($V_{C_2H_2}$=1023cm^3 V_{dopant}=998cm^3), as well as their pressures, the expression relating the pressures neccessary to achieve a desired ratio is

$$\frac{n_{dopant}}{n_{C_2H_2}} = \frac{P_{dopant}(.01)(998)}{(1023)(800)}$$

Thus, to achieve a gas mixture of 10^{-4}:1, dopant to C_2H_2, a pressure of 8.2 Torr in MC2 was neccessary.

For higher ratios, the entire mixing system was filled with C_2H_2 to some initial value. It was then filled to a second higher pressure with the dopant gas, using the same safeguard against back-diffusion as mentioned before. Using this method, the relationship between respective gas pressures and the resulting dopant concentration is

$$\frac{n_{dopant}}{n_{C_2H_2}} = 0.01\left(\frac{P_{final}}{P_{initial}} - 1\right)$$

A constraint on the choice of an initial pressure of acetylene was that the final pressure reached be above the half atmosphere limit mentioned earlier. The use of these two different mixing schemes was made neccessary by the wide range of concentrations needed,

requiring fine control of small volumes of dopant gases in some cases, while handling large amounts in others (ratios above 10^{-2}:1). Once mixing was accomplished the next step was to run the discharge.

The VS-9 pump station was then shut down, and the gas disposal system put into operation(the oven was preheated). The valve separating the mixing system from the discharge system was opened, and a stable pressure of 0.8 Torr was established, with a flow rate of 1 sccm. The Hipotronics power supply was then brought up to between 300 and 400 volts, at which time the discharge started. Startup was usually accompanied by moderate arcing for a few seconds, after which the discharge settled into a steady blue glow, localized for the most part to the region between the face of the sample and the screen cathode. Care had to be taken in regulating the discharge, as excessive voltages would result in the spread of the discharge to regions where it is not desirable, such as the base plate of the reaction tube. In addition, over-voltage could lead to arcing, causing current surges sufficient to trigger the overload detector on the supply and end the run prematurely. The discharge was run with the discharge current(i_d) between 1 and 4ma, for a period of from six to ten minutes for samples fabricated on molybdenum covered slides, and from forty minutes to one hour for samples on plain glass, sapphire, or silicon. All

these deposition times resulted in layers of a-C:H several thousand angstroms thick. Thickness was determined by establishing a correspondence between the number of diffraction fringes observed coming inward from the edge of the sample, and the thickness as determined by an optical interferometer. It was found that each fringe observed corresponded to a thickness of approximately 1500A.

Two additions to the previous discharge startup procedure were added about half way through my work. An addition to all discharges was that of a pure Ar discharge prior to carbon film deposition. This discharge was run after the initial overnight pumpdown, for a period of one minute (i_d=1 ma, P_{Ar}=1.5 Torr). After this cleaning, the system was pumped to approximately 2 x 10^{-7} Torr, at which time the regular discharge procedure was followed. This additional step served to clean the substrate surface, and alleviated problems encountered with sample adhesion in those samples prepared at low temperature(below 250C). A second modification of the discharge procedure was made by the introduction of a bakeable screen cathode. After the overnight pumpdown, the screen was baked out to remove surface contaminants. This resolved a problem encountered in depositing a-C:H on insulators. As had been noted earlier[32], and verified by myself, films of a-C:H grown in excess of one micron thickness

become unstable. When growing films on insulators, the growth rate on the substrate was far less than the rate of growth on the screen cathode. This observation seems reasonable as there is likely to be a surface charge buildup on an insulator, inhibiting deposition. Another factor here is that the substrate is no longer a source of the field generating the discharge, thus reducing the intensity of the discharge at the substrate surface. Thus, the film on the cathode screen reached an unstable thickness first, and flaked off, causing arcing and ending the run. The introduction of the heated screen resolved this problem by greatly increasing film adhesion to the screen, delaying the time at which the films flaked off, and allowing the run to proceed as a stable discharge.

Upon completion of the discharge, the entire contents of the gas mixing system were pumped out via the gas disposal system, and the entire system was purged with argon three times. The full system was then pumped below 10^{-6} Torr, and the gas mixing system was sealed off, leaving it under vacuum when not in use. The samples prepared in this manner were then removed from this system and analyzed by the methods described in the following section.

4a) ANALYSIS PROCEDURE-ELECTRICAL

Experimentation on and characterization of the electrical properties of these a-C:H films was carried out on those samples prepared on molybdenum covered substrates. Once the a-C:H film was deposited, the sample was removed from the discharge system and placed in the NRC vacuum system(Fig 2.5), where a set of 1/16" diameter molybdenum dots were deposited on the sample surface in the pattern as shown in Fig 2.6(b). The sandwich geometry formed(Mo/a-C:H/Mo) allowed the sample's conductivity (as a function of temperature) to be probed by passing a small current through the film. The use of this particular geometry was made necessary by the low conductivities encountered, in some cases as low as $\sigma \sim 10^{-16} \Omega^{-1}\text{-cm}^{-1}$.

The sample, with the Mo dots in place, was then mounted in the measurement apparatus as is shown in Fig. 2.6. The design of the substrate heater in this case was modified so that its entire front face was covered with a SS plate, again to insure uniform heating of the sample, as well as to provide good electrical contact. Once the sample was mounted, the 0.005" thick Ta contacts were lowered gently, each onto a separate dot, by sliding the Teflon block down

the 3/8" support rod. Alignment of the Ta probes with the dots was accomplished by rotating the SS rods to which the probes are spotwelded. Since the probes are bent slightly off the axis of rotation, there is sufficient lateral movement to allow proper placement. Once mounting is complete, the sample becomes part of the circuit shown in Fig. 2.7. In an effort to reduce to a minimum the spurious voltages and leakage currents introduced into the circuit, the entire face of the substrate heater is held at the test voltage(V_t) by a low impedence voltage source. The probe, and thus the electrical connections between the sample and the electrometer, are essentially at ground potential, thus preventing leakage in the connectors or in the coaxial cables between the central conductor and ground, in the same manner as it is done through the use of triaxial cabling. The NRC vacuum system, where this device was also located, was then pumped to a pressure of less than 10^{-6}Torr, at which point measurements were made.

Once under vacuum, a standard series of tests were performed before taking data. The first test was a check to insure the film was not shorted out or burned through at the site of the dot being measured. For samples produced below 350C, a simple resistance measurement sufficed, as a shorted out dot had a conductivity many orders of magnitude too high to be reasonable. In cases where there was any doubt as to

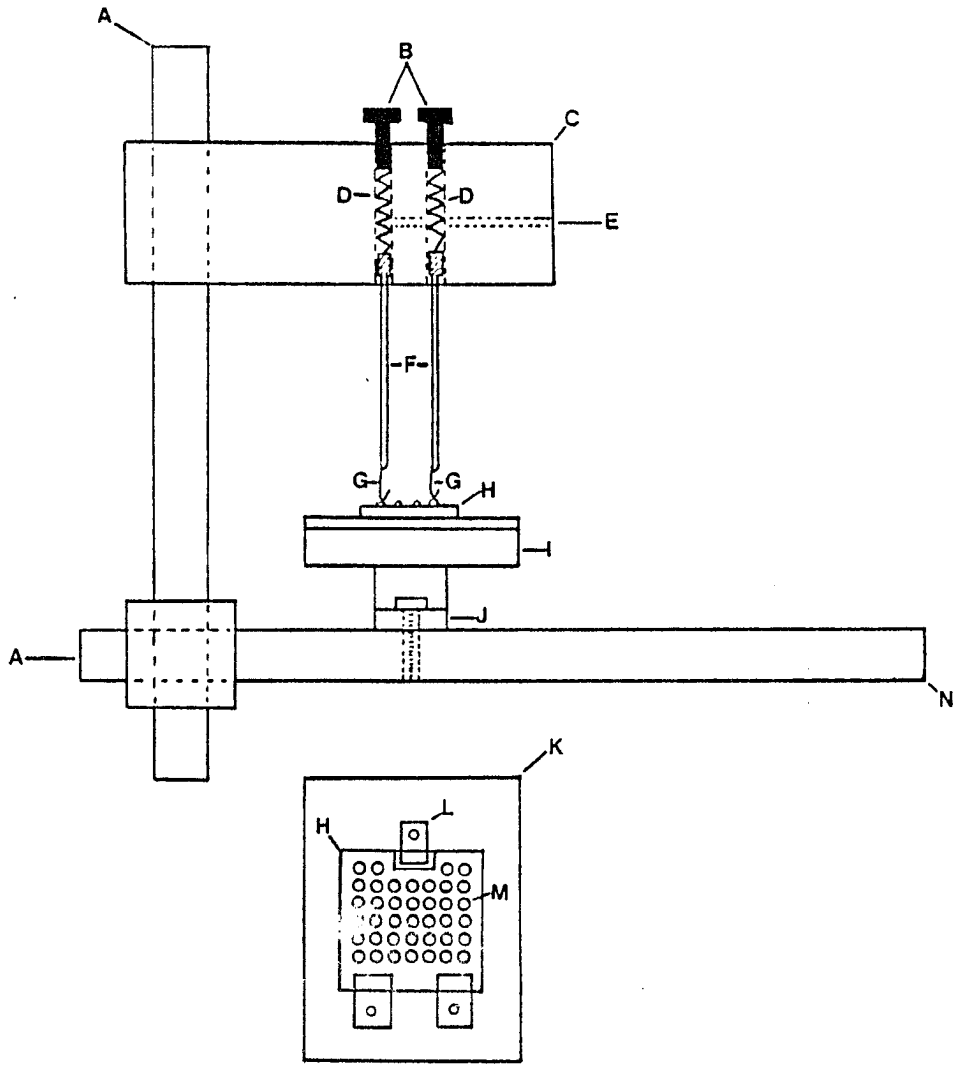

Fig. 2.6

A) 3/8" support rod B) probe pressure adjuster C) Teflon block D) spring E) air vent F)SS rod: electrial contact to Mo dot on sample G) .005" Ta contact H) sample I) substrate heater(detailed in Fig. 2.2) J) electrically and thermally insulating Macor mount K)top view of heater face L) SS clip and electrical contact to Mo layer under the a-C:H film M) Mo dots on sample face N) attached to hardware of vacuum system at this point

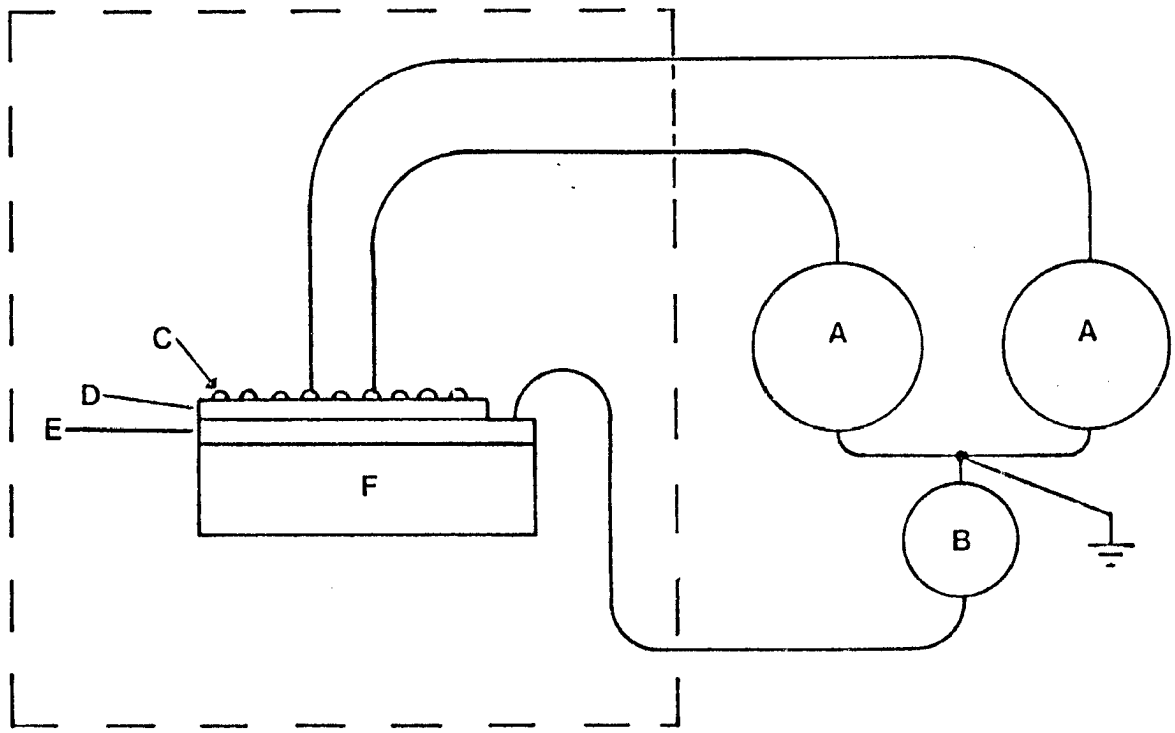

Fig. 2.7

Conductivity Measurement Circuit. A) Keithley 610C Electrometer B) Hewlett Packard 0-40volt, .5A, C) Mo dot D) a-C:H Film E) Mo layer on substrate F) Glass cover slip . The dotted line denotes the boundary of the vacuum system.

whether a reading was sensible, such as when heavily doped samples were produced having relatively high conductivities, the sample was heated, and the current at a fixed voltage was observed. If current decreased with increasing temperature as 1/T, one could be reasonably sure that the observed resistance was due to the Mo substrate, and that the dot was bad. Dot failure became much less of a problem as the quality of the Mo films on which they were being deposited was improved, emphasizing the importance of high quality deposition techniques. Film breakdown, and thus dot failure, could also be induced if stray voltages were not carefully grounded out during the setup of the experiment. After several dots failed inexplicably(no pinholes could be observed in the substrate or films), it was noticed that this only occurred when the substrate heater power supply was off during setup. Investigation showed that, when off, the supply was not grounded, resulting in a buildup of large amounts of static charge on the substrate heater. This would discharge to ground through the film when the probes were put in place, immediately burning out the dot.

A second important procedure was to check for ohmic contacts to the sample surface, as deposition of metal films on the surface of a semiconductor is a standard method for the fabrication of Schottky barriers[33-35]. This test was accomplished by

checking the I-V characteristics for each dot. It was found that for measuring voltages of less than 0.1 volt(E 2000V/cm), a plot of I vs. V was both linear and symmetric about V=0, as would be expected of ohmic contacts. Higher measuring voltages resulted in non-linear I-V characteristics, the origins of which will be discussed in the sections to follow.

These checks having been made, the sample was baked at 275C for approximately 20 minutes. This was to insure that the sample's characteristics would stabilize, as well as to remove any surface contaminants adsorbed on the sample surface that might have lead to inaccurate current readings due to large leakage currents across the sample surface. Using a typical measuring voltage of 0.1volt(E 2000V/cm), a series of measurements were then made at intervals of 10C, with the temperature decreasing from 275C to room temperature. The sample's temperature was allowed to stabilize after each interval, and spot checks were made along the way to insure that the I-V characteristic was still linear, as well as make sure that I=0 when V=0(no large offset voltages).

4b) ANALYSIS PROCEDURE-OPTICAL

In these measurements, samples prepared on glass slides were used for optical absorption measurements in the energy range of 1.6-3.6 eV. The studies, which determined E_{opt}, were performed on a GCA McPherson Spectrophotometer. The samples were mounted on a target and placed centrally in the measuring beam, and a plain uncoated glass slide was placed in the reference beam to wash out any absorptive effects due to the substrate. After calibrating the instrument for 100% and 0% transmission, a sweep of the previously mentioned energy range was made, with the resulting data on transmission analyzed as shown in the following section. For measurements made in the infrared region of the spectrum, a Perkin-Elmer Model 180 Spectrophotometer was used, and the measurements were performed on samples prepared on sapphire substrates.

To allow for effects due to reflection off the extra interfaces the beam encounted when passing through the film(the air/a-C:H interface, as well as the a-C:H/glass interface), the reflectivity of a-C:H was measured. The outcome of these trials was inserted

into the evaluation procedure to correct the absorption data for the error these factors introduced.

5) THERMOPOWER

The measurement of thermopower in highly resistive samples (those with $R \gtrsim 10^{10}$) is an especially difficult undertaking. The experimental difficulties encountered here arise from the fact that the measurement circuit will be highly susceptible to the pickup of spurious noise signals, yielding a small signal to noise ratio. Additional problems arise in this case as the magnitude of the signal being measured in a-C:H is on the order of $10\mu V/K$. Referring to the text prepared by Keithley Instruments[36] it is found that in making these measurements one is operating at the edge of the realm of feasibility(Fig. 2.8). Several factors contribute to the limit of measurement feasibility. One consideration is the need that one's voltage measurement circuit be of significantly greater impedance than that of the samples to be measured. The difficulty here is that as one employs measurement equipment of higher impedance, the resolution of such equipment declines. The maximum resolution of the Keithley 616 electrometer employed

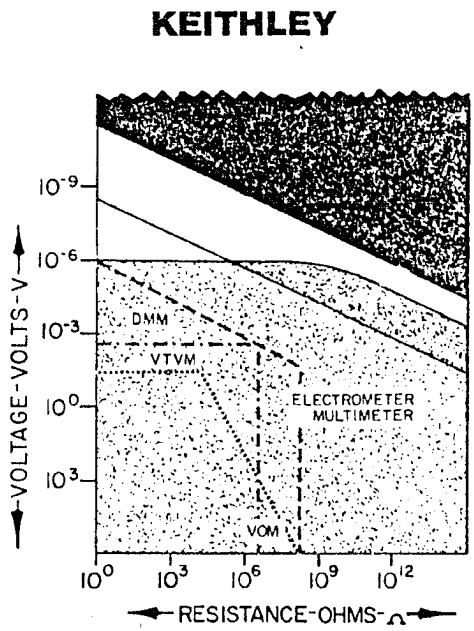

Fig. 2.8

Measurement feasibility for various devices given the source resistance and signal magnitude, as per Ref. 34.
(See discussion in text)

here was ± 10μV, the same order of magnitude as the signal observed. Zero drift of the meter adds to one's difficulties as it too is on the order of ± 10μV/°C. As ambient temperature in a typical working environment may vary by as much as 1°C/10min, the accuracy of a given measurement is reduced according to the time span during which it is taken. Thermally generated noise[36] from within a source resistance contributes a voltage signal expressed by

$$emf = (4\pi kT \Delta f R)^{1/2}$$

where Δf is the noise bandwidth in hz, and R is the source resistance. The thermal noise is used to establish an absolute theoretical measurement limit(shown as the black region in Fig. 2.8), and the other factors mentioned earlier establish the limits on the performance of each device shown in Fig 2.8. It is thus crucial that every effort should be made to shield the system from extraneous signals due either to internal or external sources.

Shielding from external sources was accomplished through the use of triaxial and coaxial leads for all cables within the voltage measurement circuit. Toward the goal of further shielding the sample, the area in which it was held was enclosed in a grounded aluminum box (Fig. 2.9), which was subsequently placed inside a

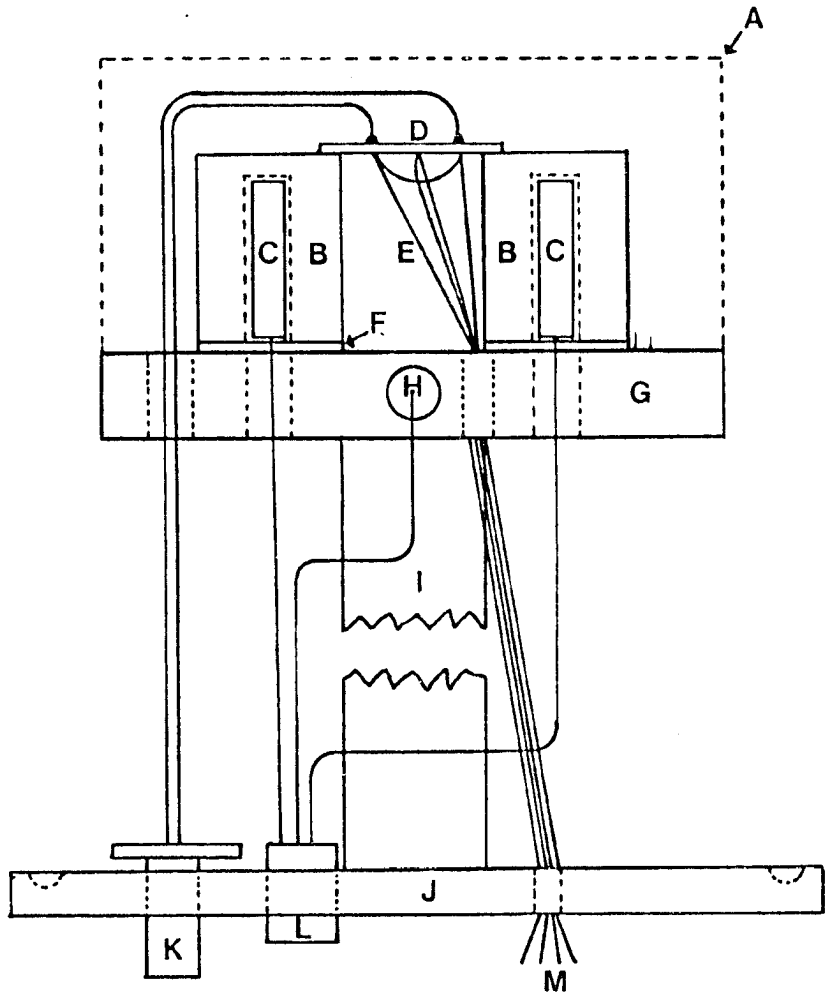

Fig. 2.9

A) Aluminum Shielding Box B) Differential Heater Blocks C) Hotwatt SC 181 15watt Heaters D)a-C:H Sample on Sapphire Substrate E) Thermocouple Leads F) Teflon Spacer for thermal isolation G) Aluminum Base Plate H) Main Heater Cartridge I) Teflon Support Pillar J) Vacuum Tight SS Plate K) Triaxial BNC Feedthrough L) Multipin Heater Feedthrough M) Thermocouple Leads

grounded steel vacuum dewar. Prior to sample measurement, the dewar was pumped down to a pressure below 10^{-6} Torr. All electrical feedthroughs into the system were made using Teflon insulated and hermetically sealed BNC connectors. As thermopower measurements are made by establishing a temperature gradient across the sample, heaters are present in the system as shown in Fig. 2.9. All cables to these heater cartridges are shielded, and the metal cased cartridges are themselves embedded in grounded brass or aluminum blocks, thus protecting the sample from stray voltages. A Power Design (0-50 volt) dc dual regulated supply is used to drive the heaters. The use of a quiet dc source is important in reducing inductive pickup. Though all of the above precautions are observed, problems will still be encountered unless the area of the experiment is kept both physically and electrically quiet. The motion of a person at a distance of five feet will cause off scale readings, and the use of a soldering tool anywhere within sight will do the same. It is thus advisable to isolate the setup as much as is possible.

In addition to noise reduction via shielding, another part of the problem involves reducing the magnitude of thermal emfs generated by junctions of dissimilar metals within the apparatus. These can be

reduced either through outright elimination of such junctions, or through the use of low thermal silver solder. These precautions are especially important if one anticipates a small signal($\sim$10uV/K), as thermal emfs may themselves be larger than this.

When ready to be measured, the sample was suspended between the two differential heater blocks as shown in Fig. 2.10. To affix the sample to the blocks, G.E. #7031 Adhesive and Insulating Varnish was used. The varnish was applied to the top inner edge of each support block in a 50% diluted form, mixed with a 1:1 solution of alcohol and toluene. This held the sample in good thermal contact with the blocks while not unduly influencing its electrical properties. The choice of this adhesive was important as it did not outgas at elevated temperatures (T=250C). Several other adhesives were utilized, and it was found that when heated, the adhesives outgassed material that was deposited throughout the system, forming conducting paths to ground and thus shorting out the highly resistive sample. Once the sample was mounted, the chromel/alumel/chromel differential thermocouple and the central temperature sensing (chromel/alumel) thermocouple were attached to the underside of the substrate as shown in Fig. 2.10. The junctions were attached to the substrate using a drop of the diluted varnish. This established good thermal contact

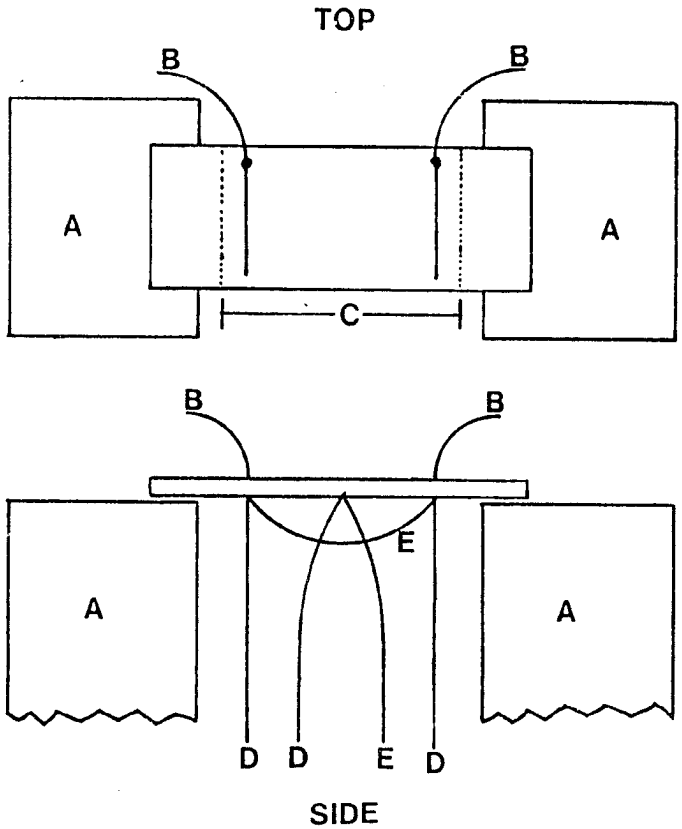

Fig. 2.10

A)Heater blocks B) Electrometer voltage leads attached to the TiAg strips under the film C) Extent of a-C:H sample on surface of sapphire substrate(1.2cm) D) Chromel thermocouple leads E) Alumel thermocouple leads Note: Current leakage occurred between leads B and D in the case of highly resistive films($R \sim 10^{11}$ohm)

between the sample and the junctions. Very fine thermocouple wire (0.003") was used here so as to prevent heat transport down the wire from significantly altering the readings obtained. Electrical connections to the sample were made using Tra-Duct 2902 Conducting Silver Epoxy. It must be pointed out that due to large electrochemical emfs present during the curing of this adhesive, it may not be possible to begin measurements until up to 72 hours have passed. Thus, though an initial offset signal of up to 0.1V may be observed in the voltage measurement circuit, this will diminish greatly or disappear entirely upon the full curing of the epoxy. The curing process may be hastened by heating the adhesive, but the epoxy must not be overheated(T$>$75C) at this time as it will outgas and consequently contaminate the sample.

As with the rest of the system, the choice of sample substrate material is extremely important. Sapphire appears to be the material of choice[36] due to its exceptionally high bulk resistivity at room temperature(10^{16}-10^{18} Ω-cm), which allows the analysis of highly resistive thin films deposited on its surface. The resistance of the a-C:H films measured fell between 10^6 and 10^{12} ohms. In most cases the sapphire functioned well, but in the limit of the higher resistance samples and operating at

elevated temperatures(T $>$ 150C), the equipment failed to obtain sensible readings due to a large noise signal. The problem was traced to the fact that the conduction process in sapphire is strongly activated[37], resulting in a rapid rise in the conductivity as a function of temperature. As the temperature rose, the electrometer high lead could couple to ground through the sapphire substrate and the thermocouple junction on the underside of the substrate(the leakage path is described in the subheading of Fig. 2.10). This was only a problem in samples where $R > 10^{11}\Omega$.

It is still possible that after all the above precautions are taken one will observe an offset voltage(a non-zero voltage measured even though the temperature gradient is zero). This may be disregarded if the temperature dependence of this offset is very weak compared to that of the sample's thermopower. A typical offset observed at 25C would be $V \leq 30\mu V$, while a $150\mu V$ offset at 250C was not uncommon. It should be noted that the temperature dependence of the offset here is $V_{offset} \leq 1.\mu V/^{o}K$. This is over an order of magnitude less than the typical thermopower observed here, and several orders of magnitude less than that observed in a-Si:H[38]. Most likely these spurious voltages are due to junctions of dissimilar materials still remaining in the circuit(ie. where the voltage leads are attached to the sample, or where they pass

through the triaxial BNC feedthrough, labeled K in Fig. 2.9)

Once the sample was mounted, the epoxy cured, and the system pumped, measurements began. Typically, one end of the sample(end A) is heated 2.5C above the other end(end B). At this point, the heater on end A is switched off and end B is now heated. The net result is that while end A is cooling and end B is rising in temperature, the ambient central temperature of the sample is roughly kept constant($\pm$1C). The shift in the gradient across the sample was read by a Keithley Microvoltmeter Model 150A attached to the relative thermocouple, so that the meter's linear output drove the x-axis of a recorder. A Keithley 616 Digital Electrometer read the thermovoltage and drove the y-axis of the recorder. The usual procedure was that a sweep of 5C was made at each given ambient temperature, i.e. end A is 2.5C hotter in the initial state, while end B is 2.5C hotter in the final state. The typical time required for the completion of a sweep was 3-5 minutes, with sweep time lengthening at higher measurement temperatures. To heat the entire apparatus uniformly so that a plot of S vs. T may be obtained, the large central heater is employed. At higher temperatures it may be neccessary to operate the central heater at some intermediate power level so as

to maintain a constant temperature during a sweep of the gradient. It is important that once the heater currents are set, they not be altered during a sweep, as capacitive coupling(between the heater and voltage measurement circuits) can result in long-lived transients. When taking a series of thermopower measurements at different temperatures, the time taken for the run should be minimized, as it has been shown[39] that significant annealing effects can occur, altering the properties of the sample during the run.

The upper temperature limit on this measurement device at present is 250C, as the Teflon components will fail at temperatures above this. If higher temperature measurements are required, Macor can be substituted for the Teflon, though it is uncertain how much higher a temperature the conducting epoxy can withstand(the specifications claim an upper limit of 130C). If one allows a $\pm 10\mu V$ error in measured voltages, the uncertainty in the value of S is $\pm 4\mu V/K$.

III) Undoped a-C:H

1) Results

The a-C:H films prepared on Mo/Glass substrates for $T_d < 200C$ were nearly transparent. As T_d increased above 200C, the samples grew progressively darker, until they were a glossy black at T_d=350C. For intermediate temperatures, interference fringes caused a variety of colorations to be observed. Films grown on glass were a faint tan, and highly transparent ($\sim$90% transmission at 6000A) when prepared at T_d=25C. As T_d approached 350C the films darkened gradually, but still transmitted more than 50% of the 6000A incident light. This trend may be observed in Fig. 3.1, where α versus E is plotted for samples prepared on glass at T_d=150C, 270C, and 350C.

Films grown on the Mo/glass substrates were in the range (0.5-1.0)μ thick, while those grown on glass were (0.2-0.5)μ thick. The films appeared to be chemically inert, as they proved insoluble in a wide variety of acids, bases, and chemical solvents. Additionally, they were found to be exceptionally hard, adherent, and resistant to scratching. Previous work[40] done on the mechanical properties of such amorphous carbon films revealed them to be of greater hardness than the best

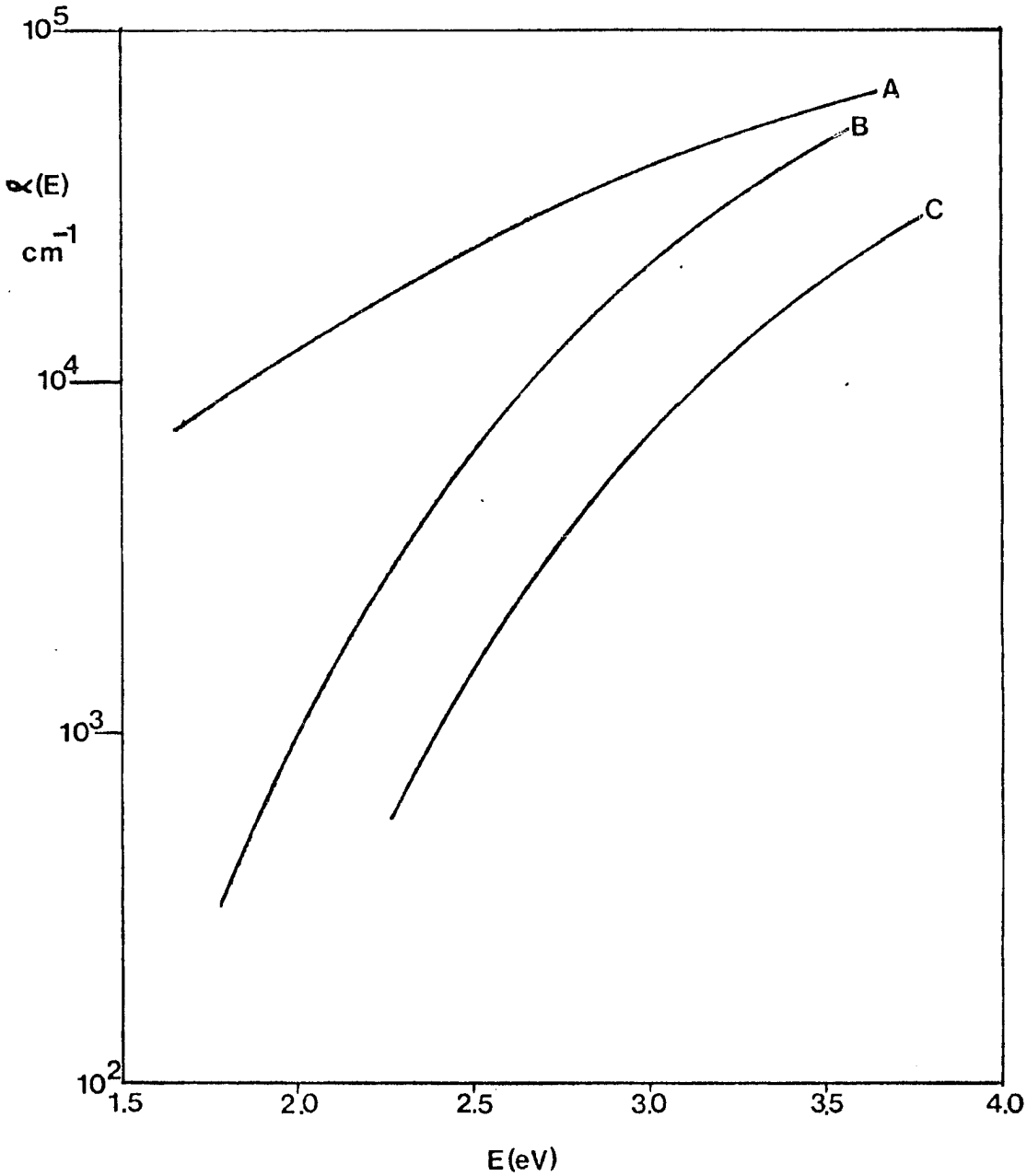

Fig 3.1

Plot of α versus E for sample A(T_d=350C), B(T_d=270C), and C(T_d=150C)

tool steels available (a Vickers hardness between 3000 and 5000). Our observation derives from the fact that while Mo surface contacts on the films were damaged or cut away during resistivity measurements, the a-C:H film beneath them was rarely damaged

Initially, films grown at T_d=25C were unstable when heated to 350C(under high vacuum) during electrical analysis. All other films remained intact during this process, though after prolonged subsequent exposure to air, films prepared with $T_d < 250C$ also deteriorated. Subsequent to the introduction of an initial pure argon discharge prior to film deposition, the problem of film deterioration was eliminated. It is likely that this discharge served to remove loosely adhered surface material such as adsorbed gas, dust, or loosely bound molybdenum surface material, thus facilitating film adhesion.

Prior to taking electrical data, a check of the current versus voltage characteristics of these films was made in order to assure that the molybdenum surface contacts were ohmic. It was found that plots of current(I) vs. voltage(V) were both linear and symmetrical about zero volts, with non-linear(though symmetric) behavior setting in when the applied field approached 10^4V/cm. Data for both the low and high field conduction regimes are presented, respectively, in Fig. 3.2 and 3.3. As the non-linear conduction data

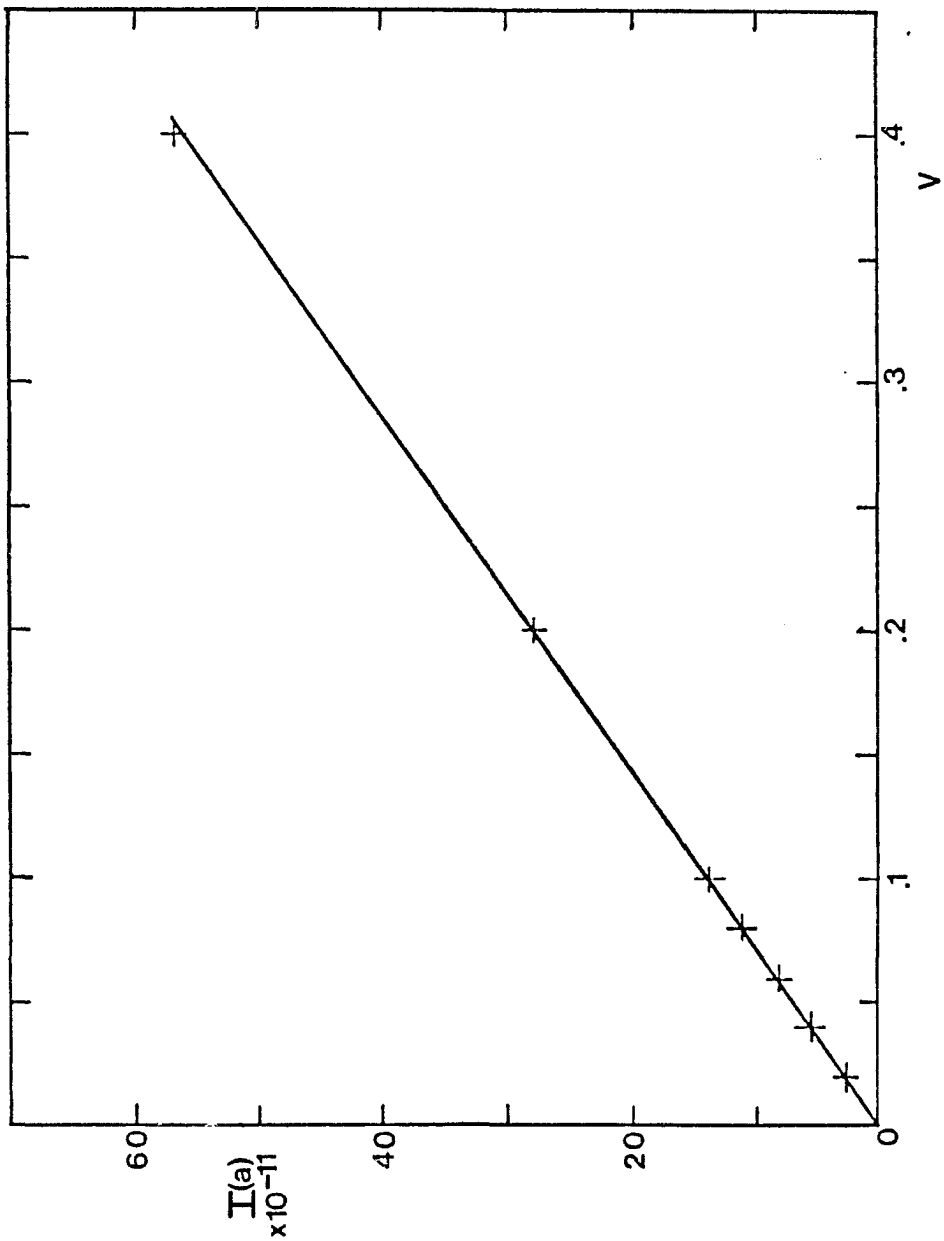

Fig. 3.2
Current(I) versus Voltage(V) data for the low field conduction regime.

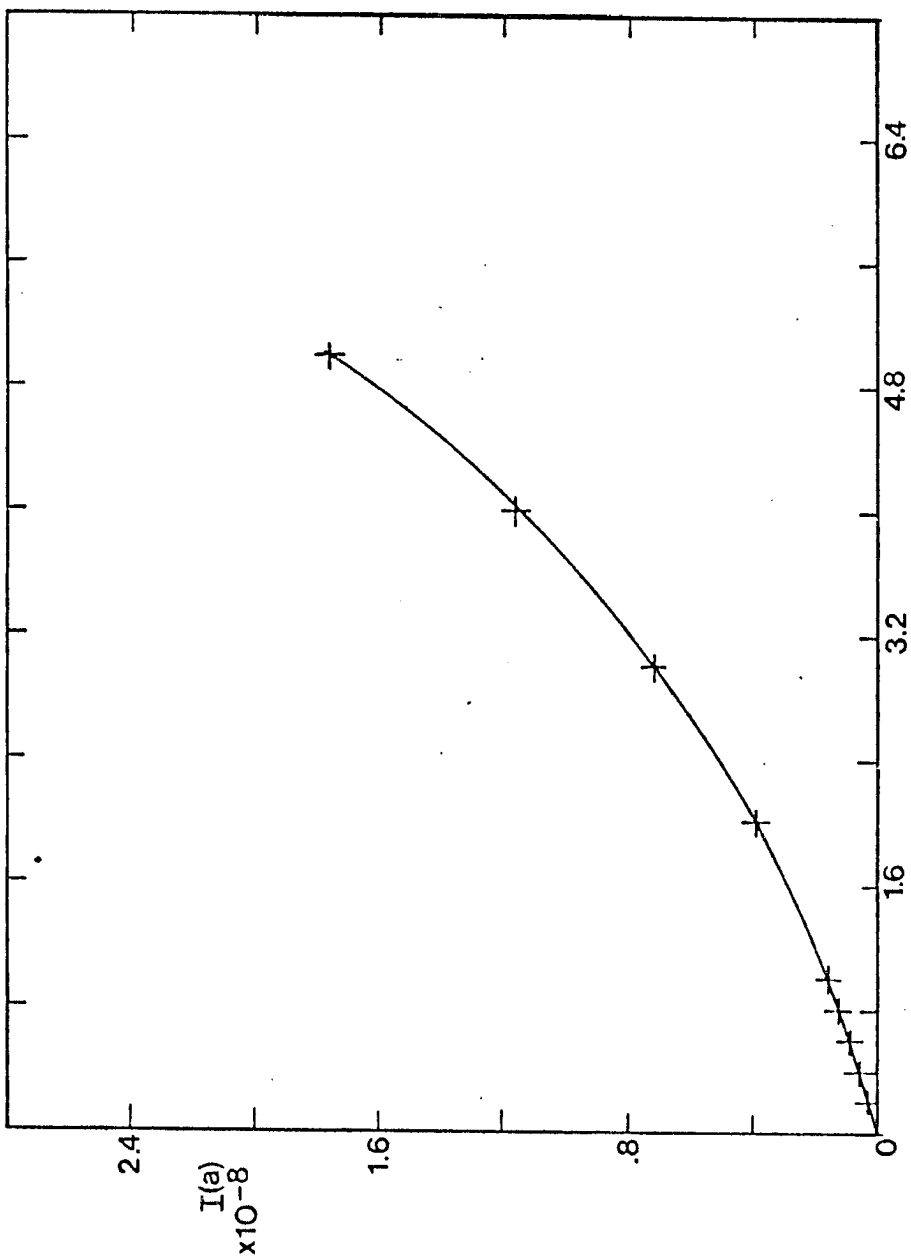

Fig. 3.3
Current(I) versus Voltage(V) data for the high field conduction regime.

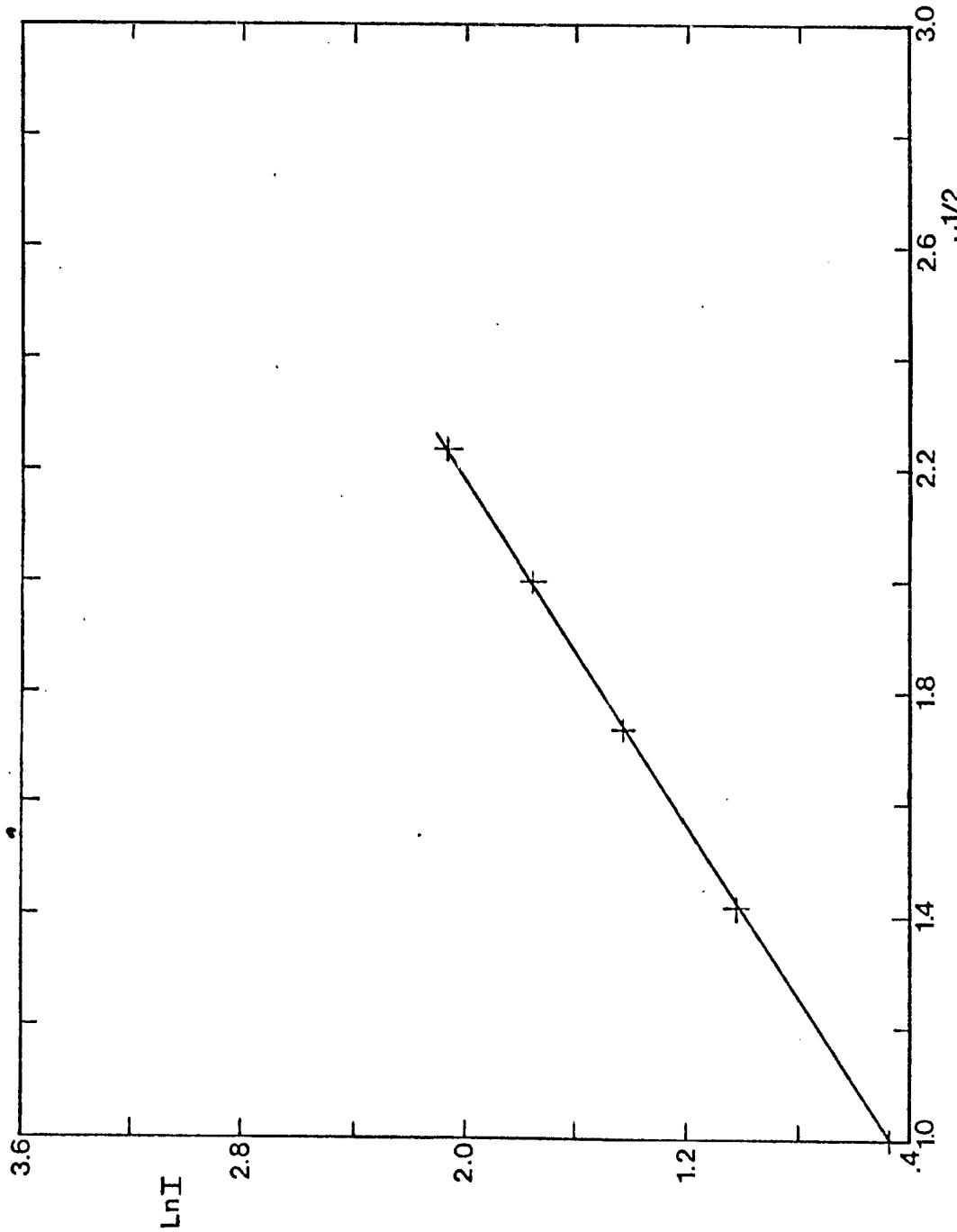

Fig. 3.4
High field conduction data plotted as a test of its fit to Poole-Frenkel theory

appeared to be field-activated, a plot(Fig. 3.4) was made of lnI versus $V^{1/2}$, the functional behavior of a Poole-Frenkel mechanism. The non-linear behavior fits well to Poole-Frenkel theory(see Theory Section).

The long-term stability of the electrical properties of these films appears to be excellent. Several films aged for a period in excess of one year in air at room temperature were remeasured, producing data virtually identical with the initial data.

Representative electrical conductivity data for these samples are shown in Fig 3.5, where $\ln\sigma$ is plotted versus 1/T. The dependence of σ on T_d is quite strong, with room temperature conductivity σ(RT) varying from about 10^{-16} to $10^{-6}ohm^{-1}cm^{-1}$ as T_d is increased from 75C to 350C(see Fig. 3.6). Except for the T_d=350C sample, does not have the simple activated form

$$\sigma = \sigma_o \exp[-E_A/KT]$$

with σ_o and E_A temperature independent parameters. As a means of systematically characterizing the curves, the two parameters $\sigma_o(250)$ and $E_A(250)$ were obtained, respectively, from the intercept and slope of tangents to the conductivity data curves at 250C. These parameters are presented as functions of T_d in Fig 3.6. $\sigma_o(250)$ is in the range $(10^{-4}$ to $10^{-2})ohm^{-1}cm^{-1}$, and is essentially independent of T_d. $E_A(250)$,

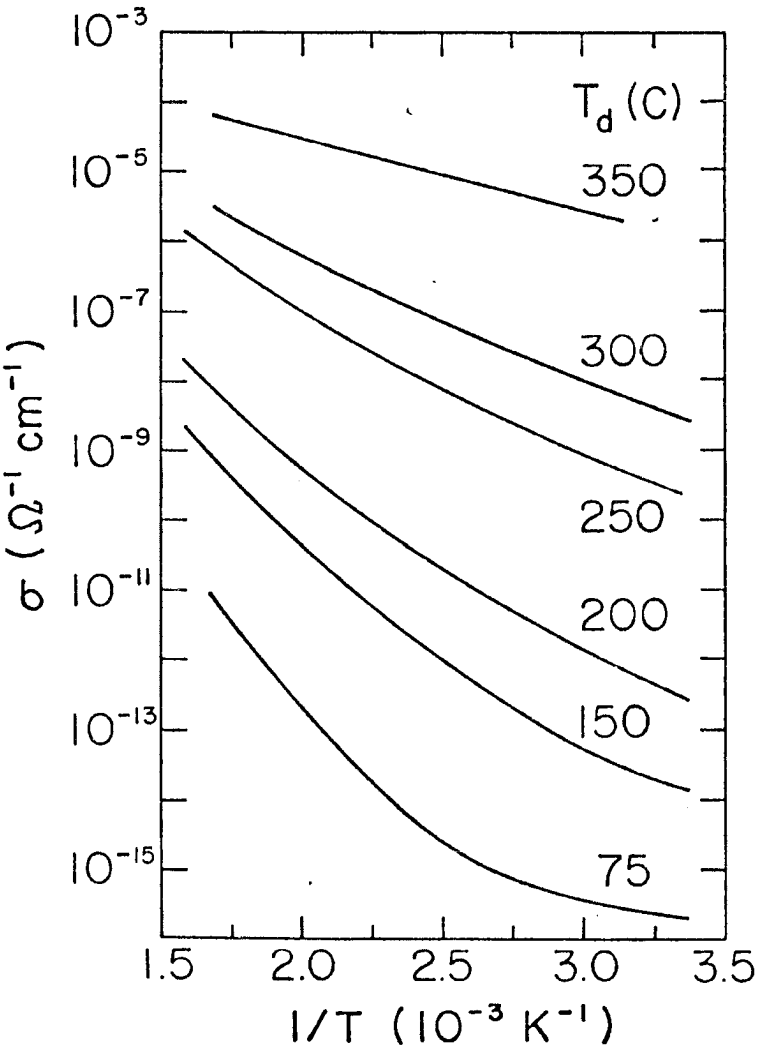

Fig 3.5

Representative conductivity data plotted for undoped samples prepared at differing deposition temperatures (T_d).

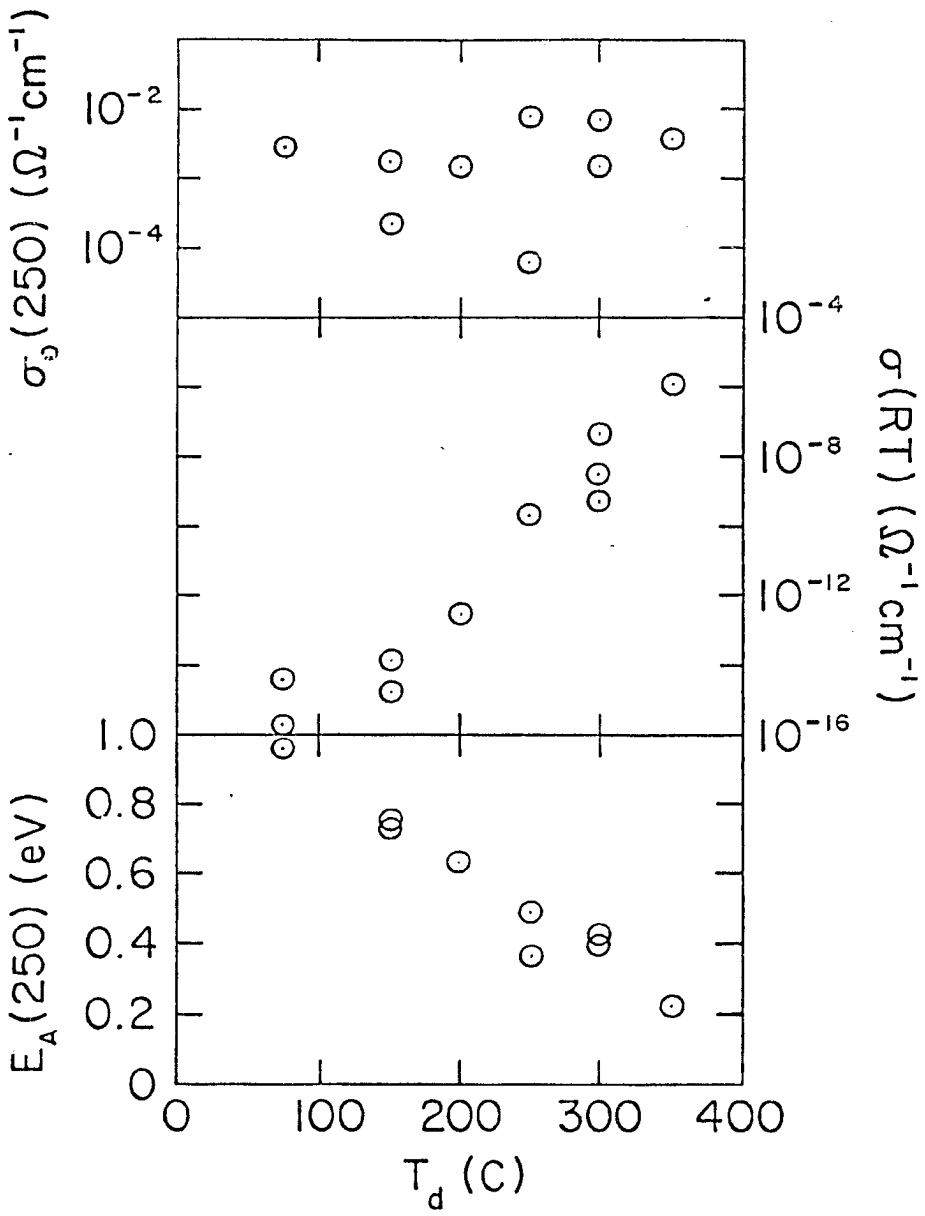

Fig 3.6

The electrical parameters plotted against sample deposition temperature(T_d). See text for definitions of $\sigma_o(250)$ and $E_A(250)$.

however, is observed to decrease essentially linearly with T_d, extrapolating to zero at about T_d=425C. Annealing the doped and undoped samples at 350C resulted in a decrease in (RT) by only a factor of two, indicating that these a-C:H films are thermally stable(in vacuum) up to this temperature.

The measured energy dependence of the optical absorption coefficient indicates that the optical absorption "edges" in these a-C:H films are quite broad. For the T_d=350C sample, $\alpha \sim 7.\times10^3 cm^{-1}$ at 1.6eV, rising to $7\times10^4 cm^{-1}$ at 3.6eV. The corresponding energies for the 270C sample are 2.5 and 3.5eV. For each sample, the optical energy gap E_{opt} has been determined by plotting $(\alpha E)^{1/2}$ vs. E as a test of the expression $(\alpha E)^{1/2}=A(E_{opt}-E)$, where E is the photon energy, and A is a constant of order $10^5 (cm\text{-}eV)^{-1/2}$. Data utilized for this purpose are corrected to allow for the reflectivity of the films relative that of a glass reference slide. A typical plot of this data appears in Fig. 3.7. E_{opt}, displayed as a function of T_d in Fig. 3.8, was obtained from the extrapolation of the linear portion of the curve to $(\alpha E)^{1/2}=0$. E_{opt} is observed to decrease from 2.1 to 0.9eV as T_d increases from 25 to 375C.

Infrared absorption studies have been performed on a variety of samples, and they indicate a strong

absorption line due to C-H bond stretching modes near 2900cm^{-1}, with little or no absorption due to C=O bonding observed in the region of 1700cm^{-1}. Absorption due to C-H bending modes was found at 1400cm^{-1}.

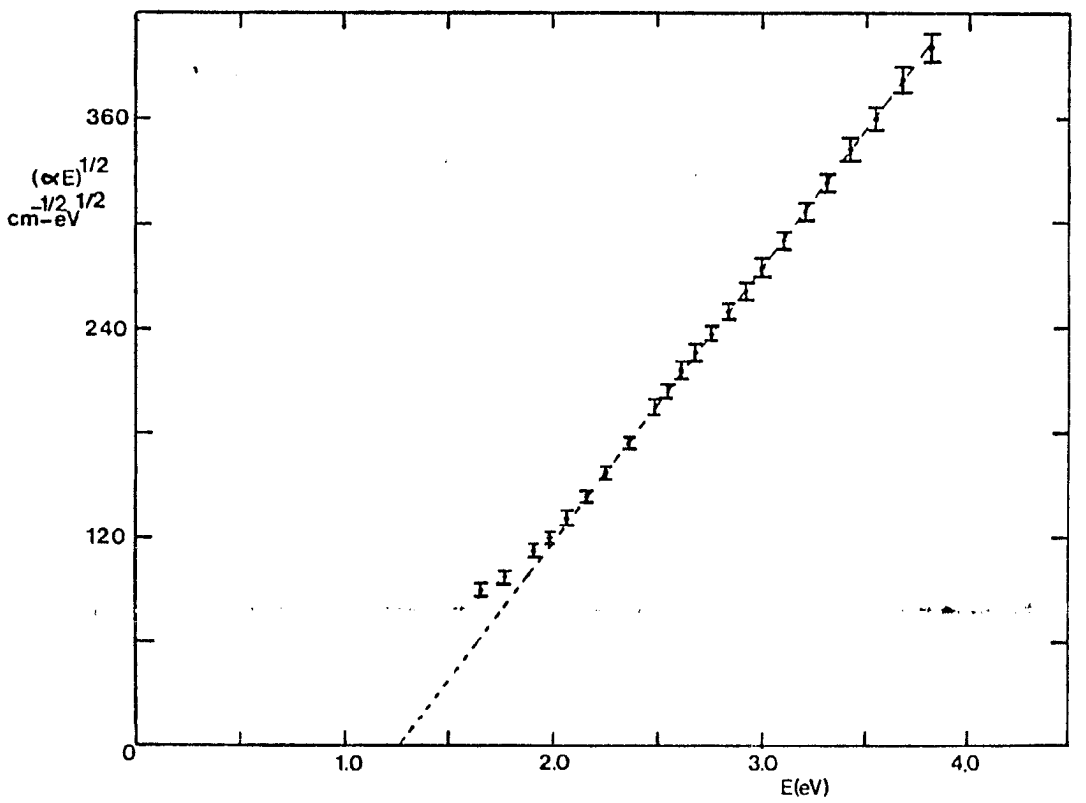

Fig. 3.7

Optical absorption data for a sample prepared at T_d=350C. See for comparison Fig. 3.1 .

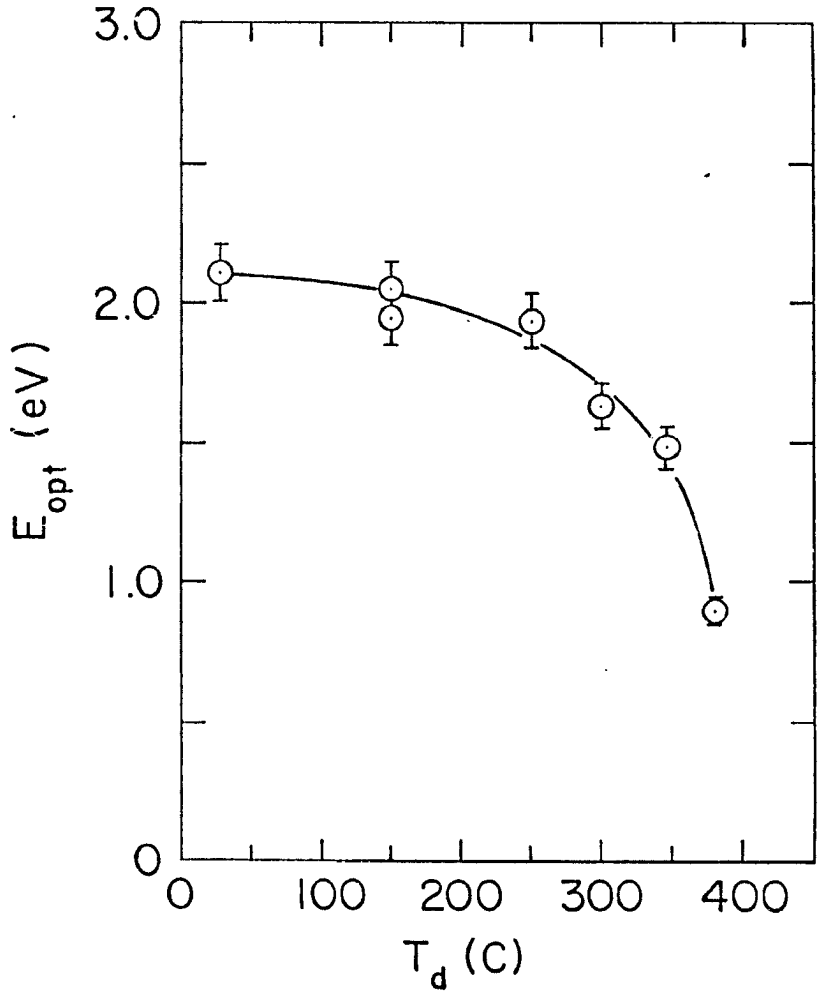

Fig. 3.8

Optical gap(E_{opt}) plotted against sample deposition temperature(T_d).

2) DISCUSSION

For the semiconducting films studied, with T_d between 75C and 300C, the curvature of the log σ vs. 1/T plots, as well as the low values obtained for $\sigma_o(250)$, would seem to preclude an interpretation of this conduction process as being extended state conduction taking place beyond the mobility edges in either the conduction or valence band. In addition, the conductivity data are not consistent with variable range hopping near the Fermi energy E_F, as plots of log vs. $T^{-1/4}$ are not linear[9h]. A self consistent picture of the conductivity data may be obtained by viewing the conduction mechanism as involving carrier excitations into a broad range of localized states near one of the band edges, where the conduction process would occur via thermally activated hopping.

It would be reasonable for the observed curvature in the plot of ln σ vs. 1/T to result if additional states, either initial or final, became accessible to thermal activation as temperature rose. Such a broad band of tail states is consistent with the results obtained during the optical absorption studies, which indicated that the optical edges were broadened out.

If the conduction process took place solely via nearest neighbor hopping within the tail states of the mobility gap, the expression describing this case would be

$$\sigma = \sigma_o \exp[-(E_A - E_F + W)/kT]$$

as shown in section I (eqn I.6). To arrive at this expression, it was necessary to assume a linear tailing off of the conduction band into the gap, with an arbitrary limit set on the extent of the tailing. It is apparent, from the dependence of σ_o and E_A on measurement temperature, especially evident in those samples prepared at $T_d \leqslant 300C$, that some mechanism in addition to conduction in a band tail may also be operating here. As this material appears to have a significant density of states well within the mobility gap, a plausible explanation of the observed curvature may be obtained by considering a variable range hopping regime about E_F as the competing process. As additional thermal energy becomes available, the conduction process shifts to higher energy tail states within the gap, which is consistent with the observation of an increasing slope as seen on the plots of $\ln\sigma$ vs $1/T$ in Fig. 3.5, for data taken at the higher measurement temperatures.

In Fig. 3.4, the fit of the high field conduction data to a Poole-Frenkel type expression is

excellent. Applying the analysis procedure utilizing the Poole-Frenkel theory outlined in section I, the value ϵ=1.7 was obtained. Using the simple form of $n=(\mu\epsilon)^{1/2}$ with μ taken as unity, $n\sim 1.4$. This is in fair agreement with the value($n\sim 1.7$) obtained via direct measurements of the reflectivity of these films, and a value of n~1.65 computed using our correlation of one set of interference fringes to 1500A film thickness. The agreement here is satisfactory at best, as the parameter m, discussed earlier, is an unknown quantity for a-C:H. In this calculation I used the value m=1.5, the most commonly observed[20] value when probing other low mobility semiconducting materials. However, as m=1.3 would have yielded an exact match between the observed and calculated values of n, and as 1.3 is well within the range of allowed values, this result is not unreasonable.

As T_d increases above 250C, E_{opt} drops rapidly, signalling the onset of fundamental changes in the bonding and band structure in these a-C:H films. Such changes would result from a decreasing incorporation of hydrogen at higher T_d, a well established[41] pattern for a-Si:H. With less hydrogen present, the fraction of three-fold as opposed to four-fold coordinated carbon atoms would be expected to increase. By analogy

with the fully three-fold coordinated form of solid carbon (graphite), with zero energy gap, and the fully four-fold coordinated form (diamond), with a 5.4eV energy gap, it is not surprising that E_{opt} should decrease if three-fold coordination indeed begins to dominate for $T_d > 250C$.

It is of interest to compare the electrical and optical properties of the a-C:H films prepared via the dc glow discharge decomposition of C_2H_2 with amorphous carbon films prepared via either evaporation or sputtering[42]. Evaporated and sputtered amorphous carbon films, prepared without intentional incorporation of hydrogen, have been found to have, in part, a graphitic structure[43] indicating a tendency toward trigonal (3-fold) coordination of the carbon atoms. The room temperature conductivity of these films (10^{-3}-$10^{2}\Omega^{-1}cm^{-1}$) is comparable to that of high quality graphite(σ(a-axis) $10^{4}\Omega^{-1}cm^{-1}$, σ(c-axis) $1.\Omega^{-1}cm^{-1}$). For the a-C:H films studied here, we note that $E_A(250)$ extrapolates to zero at T_d=425C (Fig. 3.6), and σ(RT) extrapolates to $10^{-2}\Omega^{-1}cm^{-1}$ at T_d=440C (Fig. 3.6). E_{opt} also extrapolates to zero near T_d=425C (Fig. 3.8). Thus, for $T_d \gtrsim 425C$, one expects to find that these amorphous carbon films would be "graphitic" as far as their electrical and optical properties are concerned,

presumably due to the reduced incorporation of hydrogen resulting in the dominance of three-fold coordination within the films.

Anderson[6] has undertaken an investigation of the electrical and optical properties of amorphous carbon films prepared by rf glow discharge of C_2H_2. My results for E_{opt}, although consistently (0.4-0.6)eV lower than Anderson's, are similar to his in their dependence on T_d. A possible explanation of these lower values of E_{opt} is that the a-C:H films prepared via the rf discharge technique used by Anderson contain more hydrogen than those prepared by my dc technique. Further evidence consistent with such an explanation comes from Anderson's electrical conductivity data, which also show curvature on a $\log \sigma$ vs. 1/T plot. In particular, his σ(RT) values are 3 to 5 orders of magnitude lower than those observed here for films prepared at the same T_d, which again is consistent with there being a higher concentration of hydrogen in Anderson's samples.

IV) DOPED a-C:H

1) RESULTS

The physical characteristics(hardness, resistance to chemical attack, transparency) of the doped a-C:H samples showed no marked dependence on dopant concentration, and were similar to those reported in section III.1 for undoped samples. The time required to achieve a given sample thickness was increased due to the presence of Ar as the dopant carrier gas, but deposition times remained in the neighborhood of 6 to 10 minutes. During the analysis procedure, which included a 30 minute anneal at 275C(to stabilize the electrical properties of the films) prior to measurement, all films were stable, and remained so after removal from the system.

As observed in the results for section III, plots of ln versus 1/T(presented for various dopant concentrations in Fig. 4.1 and 4.2) were non-linear, and it is thus evident again that there are competing transport mechanisms involved. $E_A(250)$ and $\sigma(RT)$ (room temperature conductivity), as defined in section III.1, are the parameters used in describing the electrical behavior of these films, and are plotted as functions of dopant concentration in Figs. 4.3 and 4.4.

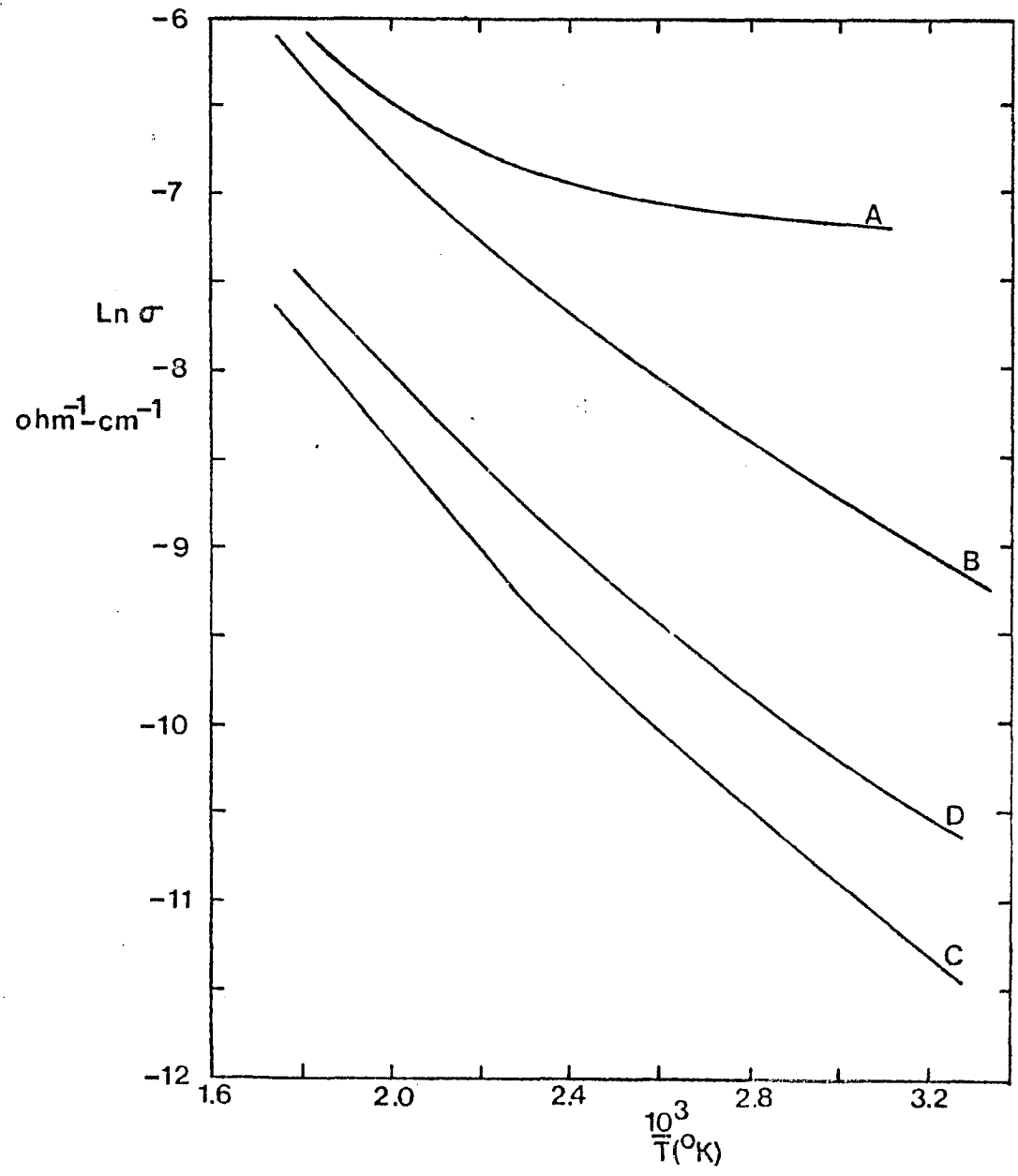

Fig. 4.1

Plot of Ln σ vs. $10^3/T$ for boron doped samples with T_d=250C. The ratios of B_2H_6/C_2H_2 for each sample are as follows; A(10^{-1}), B(10^{-2}) C(3.1×10^{-3}), D(0).

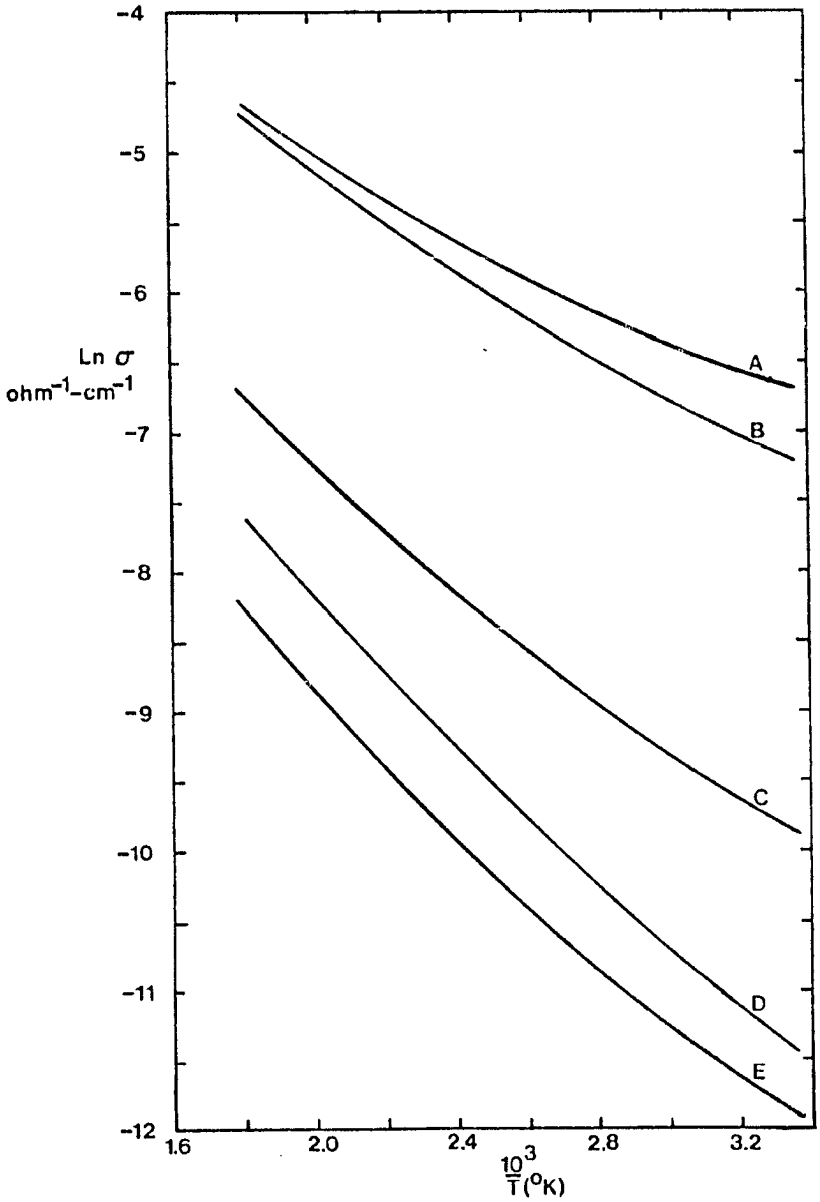

Fig. 4.2

Plot of Ln σ vs. $10^3/T$ for phosphorous doped samples with T_d=250C. The ratios of PH_3/C_2H_2 are as follows; A(2×10^{-2}) B(10^{-2}), C(6×10^{-3}), D(3.17×10^{-3}), E(0).

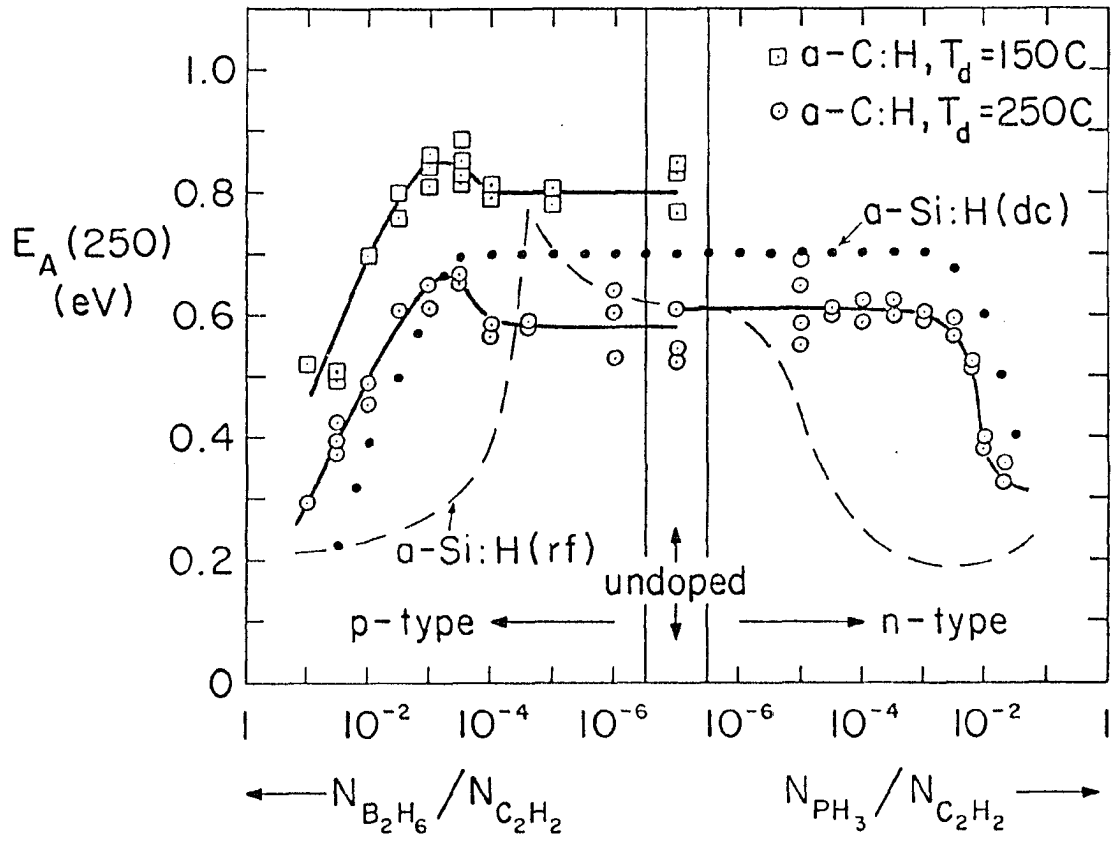

Fig 4.3

E_A(250) plotted as a function of dopant gas concentration in the discharge.

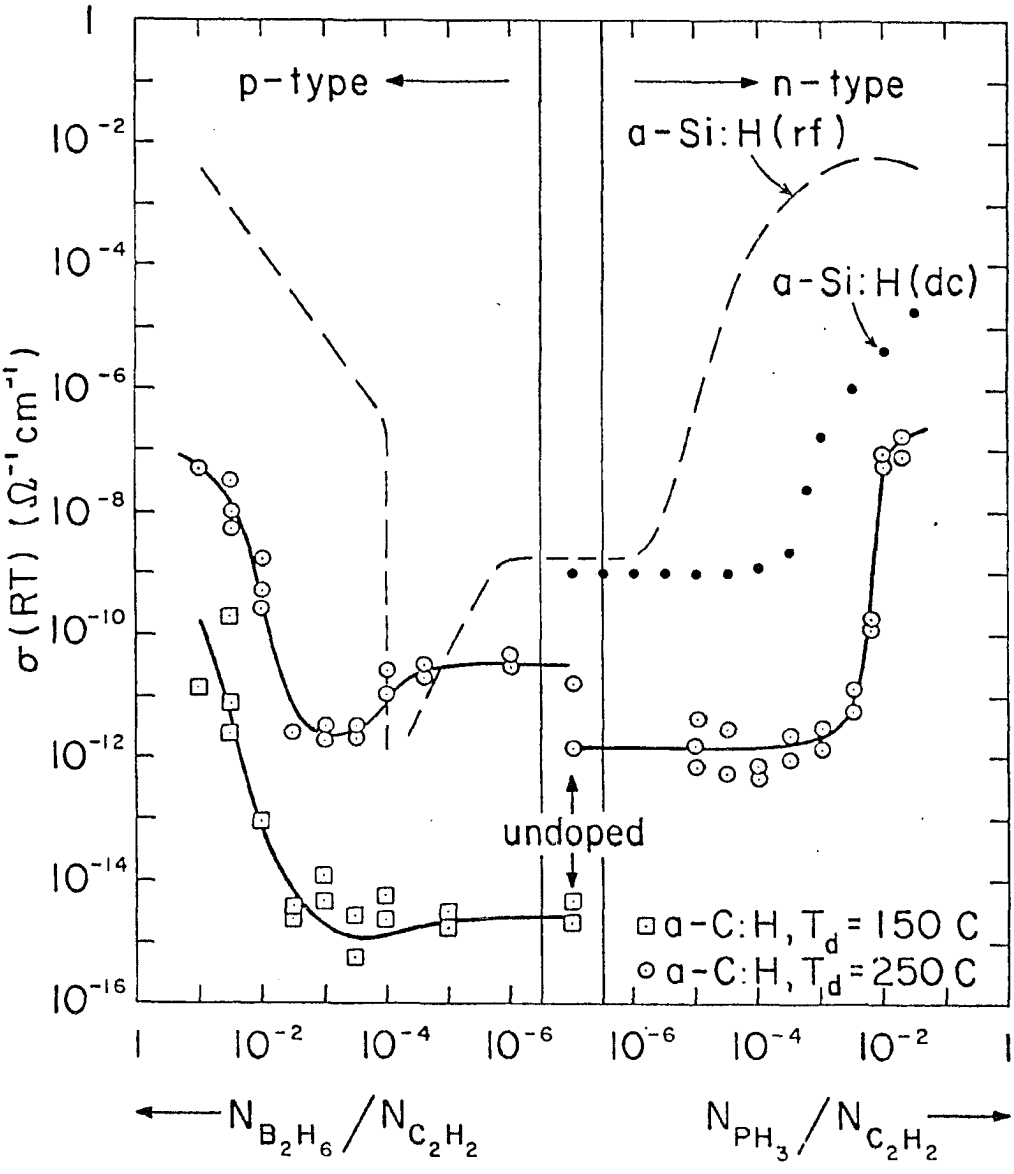

Fig 4.4

(RT) plotted as a function of dopant gas concentration in the discharge.

The values of $\sigma_o(250)$ observed here were comparable to those found for the undoped samples, on the order of $10^{-2}ohm^{-1}cm^{-1}$. Data are presented for a-C:H samples prepared at T_d=150C and T_d=250C. Similar data representing the results of doping experiments(also using PH_3 and B_2H_6) on dc[44] and rf[2] glow discharge produced a-Si:H films are included in the figures, as important parallels may be drawn between the various set of data.

The plots of $ln\sigma$ versus 1/T shown in Fig 4.5 represent conductivity data on samples prepared at T_d=325C for use in the thermopower measurements. $E_A(250)$ for the doped samples was in the range of 0.02eV for samples prepared with 2.0% diborane, to .06eV for samples prepared at 1.0% phosphine. The undoped sample yielded conductivity data in good agreement with that obtained for undoped T_d=325C samples prepared earlier, though the thermopower sample was prepared on sapphire rather than the Mo/glass substrates used previously.

The magnitude of the thermopower for these doped a-C:H samples prepared at T_d=325C and measured here was in the range (10-60 μV/K). The use of such heavily doped high temperature samples was a

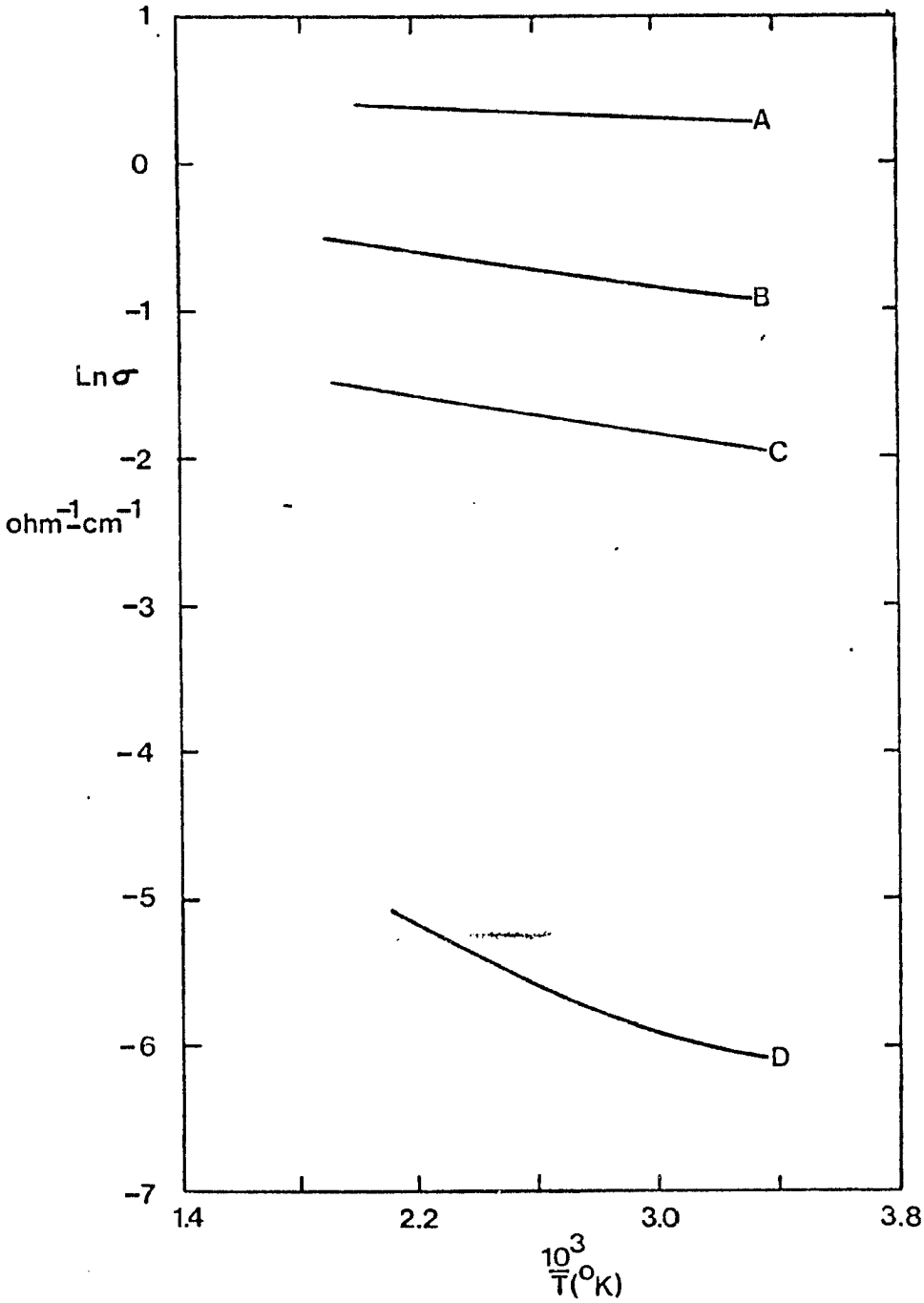

Fig. 4.5

Ln σ versus 1/T for samples prepared at T_d=325C, with percent dopant concentrations as follows A) 2.% Diborane B) 1.% Diborane C) 1% Phosphine D) undoped

neccessity as samples prepared at either a lower value of T_d or at lower dopant levels had resistivities sufficiently high to preclude the taking of reliable data(see section II for more detail). The room temperature resistivities observed in these films ranged from 10^7ohm-cm for an undoped sample, to 10 ohm-cm for one where the discharge gas (excluding argon content) was 2.0% dopant/98.0% C_2H_2.

Of primary importance here was the determination of the sign of the thermopower for those samples which had been doped. The results of these measurements are presented in Fig. 4.6, where the data are presented in the form of a plot of S versus T. The boron doped samples displayed a thermopower S that was clearly positive. The magnitude of S observed for samples doped at 2.0% B_2H_6/98.0%C_2H_2 varied from 20 to 50 μV/K as T varied from 25 to 250C. The Peltier coefficient, eST, was found to be 0.006eV for the sample prepared with 1.0% phosphine, and 0.01eV for the sample prepared with 1.0% diborane, both these values computed at T=400K.

Considerable "annealing" effects were evident in these measurements, as a consequence of which data were taken after an initial ten minute 250C anneal. This effect was observed in all the samples measured here. It was found that after a large initial effect

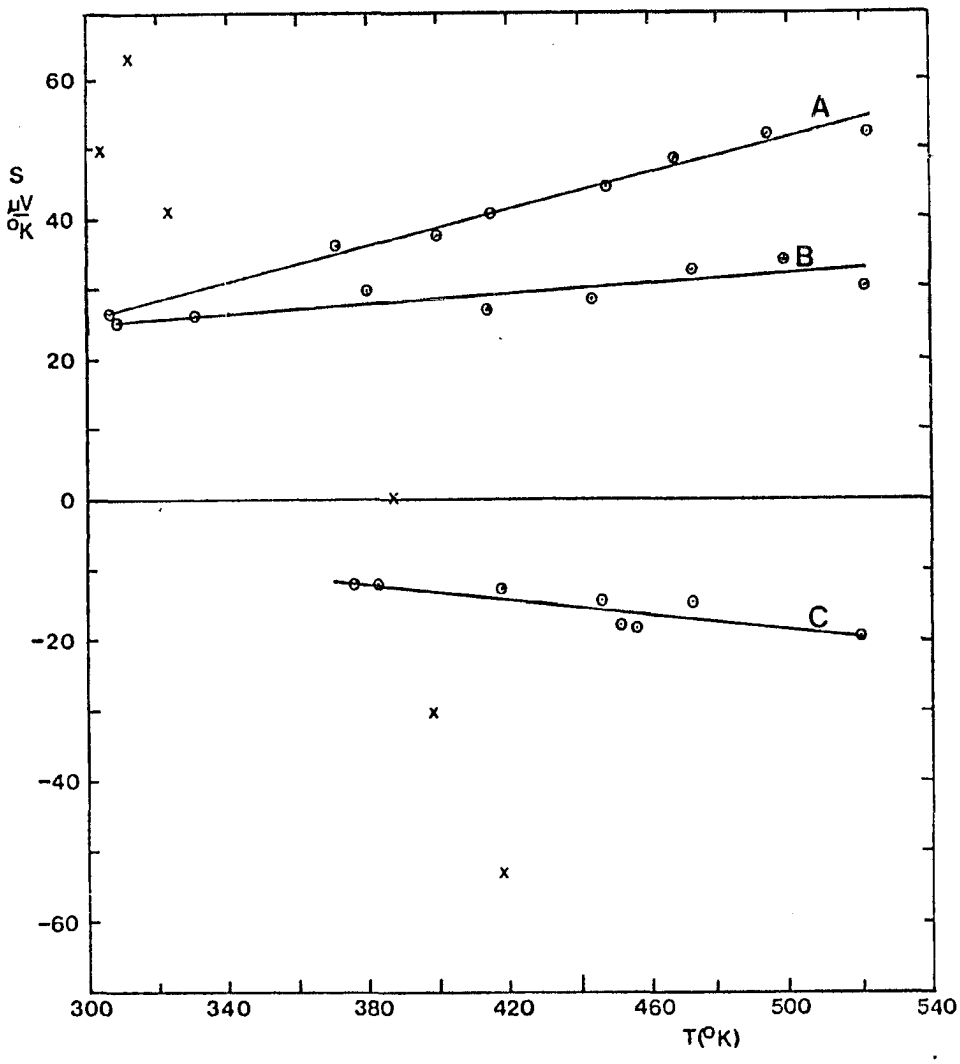

Fig. 4.6

S versus T plotted for samples prepared at T_d=325C with dopant concentrations(percent dopant in discharge gas) as follows: A) 2.0% Diborane, B)1.0% Diborane, C) 1.0% Phosphine, X) Undoped

(typically S varied by 50%), electrical properties varied little during subsequent measurements. It is conceivable that this "annealing" effect was in reality due to adsorbed surface material being removed by heating in a vacuum, rather than by an actual modification of the film's inherent properties. As a concession to these observed effects, the measurement time was kept to a minimum, in an effort to reduce the time a sample was held at elevated temperatures.

Samples doped with PH_3 displayed a negative thermopower. During an initial measurement run prior to annealing, the thermopower was positive, but rapidly went negative upon heating. Subsequent to this initial run, the thermopower remained negative. This followed a universal trend among the samples measured wherein the slope of the S versus T plot became more positive subsequent to the initial run.

Optical absorption measurements made on these thermopower samples showed the optical gap E_{opt} was within experimental error of E_{opt} obtained from the samples prepared earlier on glass.

2) DISCUSSION

From the observed shift of $E_A(250)$ as a function of dopant concentration, for both the n- and p-type doped films prepared at T_d=250C, it is inferred that the Fermi Level E_F is shifted via doping by a total of 0.7eV through the energy gap. For these T_d=250C films, σ(RT) is observed to vary between 10^{-12} and 10^{-7} ohm^{-1}-cm^{-1} for both n- and p-type doping. For the T_d=150C p-type films(n-type films were not prepared at T_d=150C), σ(RT) increased from about 10^{-15} to 10^{-10} ohm^{-1}-cm^{-1}. For both sets of films, the values of σ_o(250) fell in the range 10^{-3} to 10^{-1} ohm^{-1}-cm^{-1}, with no systematic dependence upon dopant concentration.

To check that the addition of increasing amounts of argon to the discharge(via the 99%Ar-1%dopant gas mixtures) was not responsible for the effects attributed to doping, the conductivity of a control sample, prepared from 24%C_2H_2-76%Ar, was examined. This is the C_2H_2/Ar ratio appropriate for a dopant gas/C_2H_2 ratio of 3.17%. The results obtained for this sample were the same to within experimental error as those prepared from pure acetylene under like conditions. It may therefore be concluded that the doping effects observed were indeed due to the dopant rather than the presence of Ar in the discharge.

An additional doped control sample(0.3% dopant), prepared at T_d=250C on glass, was subjected to optical absorption studies. The results showed that the optical gap was unaffected by the presence of dopant within the sample, verifying that observed shifts of E_A toward smaller values were not due to a smaller energy gap in the doped samples.

From the plots of $E_A(250)$ and $\sigma(RT)$ versus dopant concentration in Fig 4.3 and 4.4, it can be inferred that undoped a-C:H films prepared at 150C and 250C are intrinsically n-type. The initial rise in $E_A(250)$ at low diborane concentrations indicates a downward shift of E_F towards the center of the gap, followed by its continued shift towards the acceptor states established by the incorporated boron atoms. At the same time, $\sigma(RT)$ for the boron doped T_d=250C films drops by approximately one order of magnitude, from 10^{-11} to 10^{-12} ohm^{-1}-cm^{-1}, before increasing to $10^{-7}ohm^{-1}$-cm^{-1} at higher diborane concentrations. This behavior for both $E_A(250)$ and $\sigma(RT)$ is similar to that observed in the rf glow discharge prepared films[2] of a-Si:H, which are also intrinsically n-type when undoped. Further evidence of the validity of this interpretation of the data on doping will be presented later in this section when the results of thermopower measurements will be discussed.

The data presented in Fig. 4.3 and 4.4 indicate that the doping efficiencies achieved with these dc glow discharge produced a-C:H films are quite similar to those obtained in a-Si:H films prepared under similar conditions[44] (corresponding to the data labeled a-Si:H(dc) in Fig 4.3 and 4.4). Rf produced films[2] (labeled a-Si:H (rf) in Fig 4.3 and 4.4) have exhibited doping efficiencies about two orders of magnitude higher than those we observed. The production of doped a-C:H films by rf discharge techniques would be interesting, as studying the cause of any variation in doping efficiency(rf vs. dc) would yield valuable information as to the mechanism of dopant incorporation.

As discussed in section I, the doping efficiency of a semiconductor gives one an opportunity to develop an approximate representation of the gap state density of the material. Using the technique described in section I.5, the result appears in Fig. 4.7 . Several qualifications must be made here, the first pertaining to the relative doping efficiencies of boron and phosphorous. This computation is based upon the dopant concentrations present in the discharge gas, and the assumption that a constant fraction of this dopant is substitutionally incorporated into the material. The relative efficiency of boron versus phosphorous incorporation into a-C:H is an unknown, and thus forces a reliance upon what is known about this phenomenon in

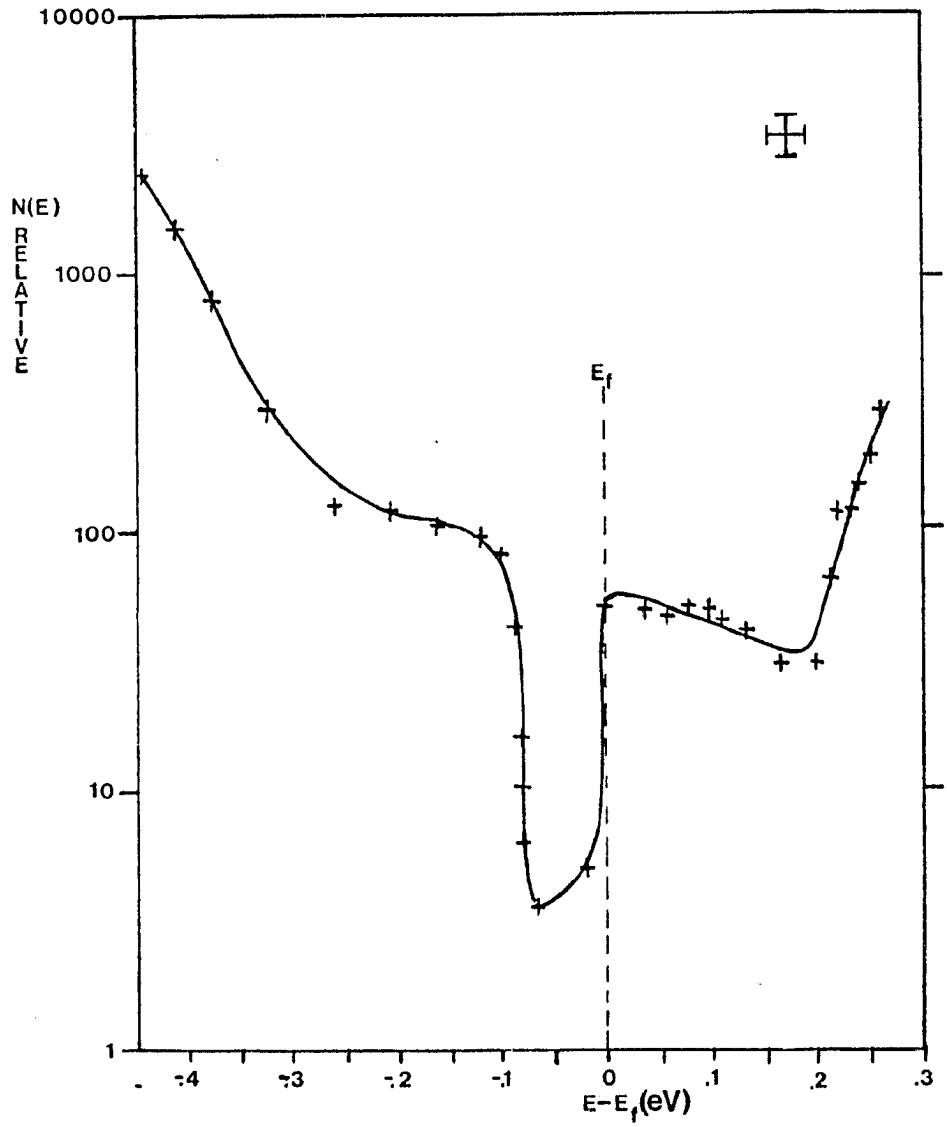

Fig 4.7

Relative gap state density in a-C:H derived from doping efficiency. The error bars(in the upper right hand corner) arise from uncertainties in both dopant concentration and the measured value of E_A, as well as from the thermal broadening of E_A.

a-Si:H. a-Si:H has been found to incorporate phosphorous as much a an order of magnitude more efficiently than it does boron[45]. Consequently, it is possible that the side of the curve closer to the conduction band should be shifted upwards to allow for this phenomenon. Though such relative offsets may occur, the basic feature of a central minimum in the density of states will be unaffected. The sharp depression in the central region of the gap state density plot must be regarded with caution, as this is a region of maximal uncertainty due to low dopant concentrations as well as the accompanying small shifts in E_F.

The placement of E_F within the gap is based upon the extent to which it was shifted in the limits of high n- and p-type dopant concentrations. To give a picture of where this central gap state region lies in reference to the mobility edges, data on the optical gap of a sample produced at T_d=250C are used in combination with the gap state density plot to give the schematic presented in Fig. 4.8 . As the onset of strong optical absorption is assumed to occur when transitions between the mobility edges take place, the overall dimension of the gap region of this material is taken as E_{opt}=2.1eV. The large difference between the amount E_F may be shifted within the gap and E_{opt} is indicative of large band tails extending deep within

the gap. The assignment of a symmetrical dimension of 0.7eV to each band tail was an arbitrary choice, though the overall dimension of the gap(2.1eV) is dictated by E_{opt}.

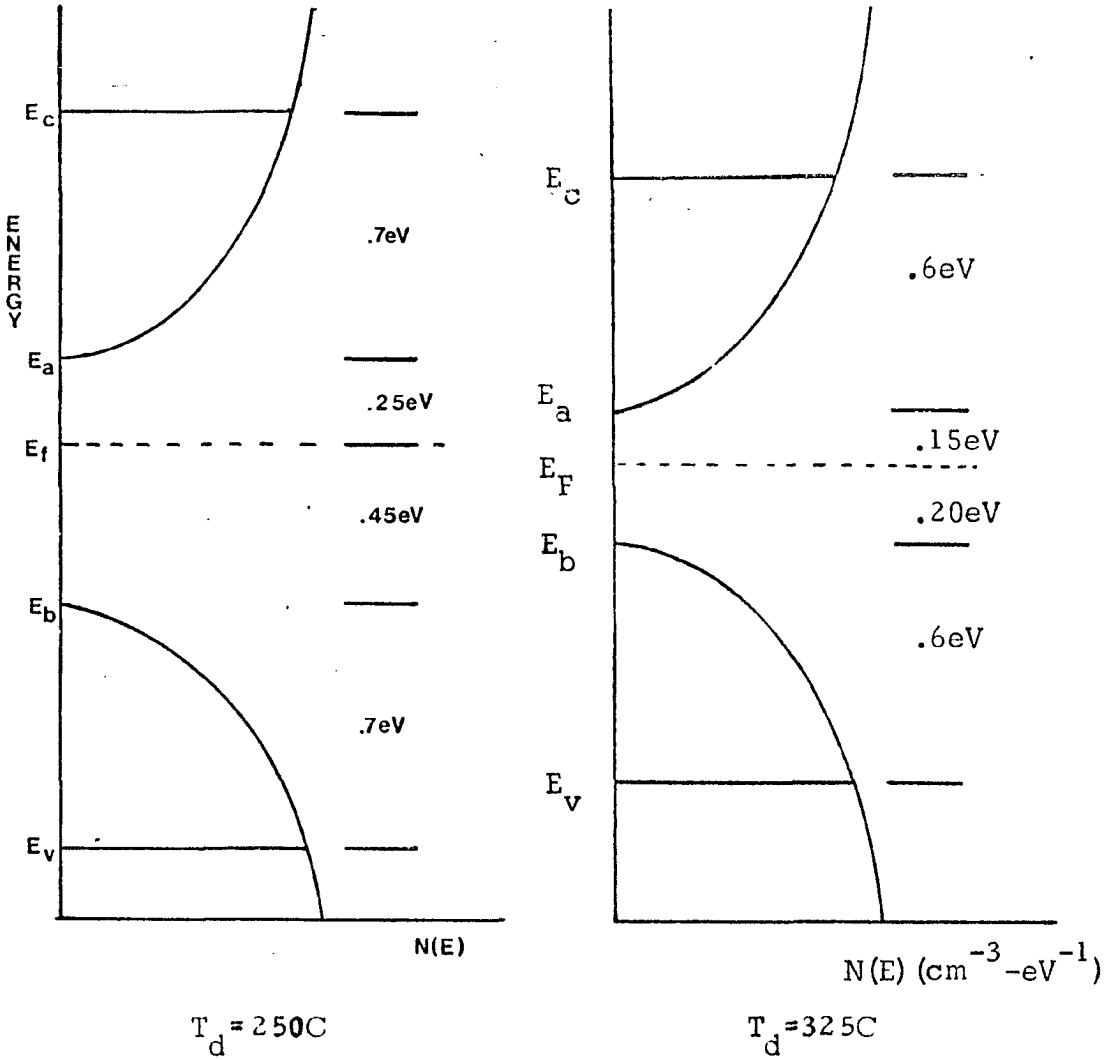

Fig 4.8

Schematic representation of the gap state dimensions of a-C:H.

The undoped samples(T_d=325C) prepared for use in thermopower measurements yielded conductivity data in good agreement with previously prepared samples, though the deposition rate of a-C:H on sapphire falls off by approximatly one order of magnitude relative to the rate for deposition on a conducting substrate(used in earlier experiments). Thus, it may be concluded that the electrical properties of these films are relatively insensitive to deposition rate as well as substrate type. The electrical properties of these films were determined by passing a current along the films between two TiAg contacts, rather than passing a current through the films as done when using conducting substrates. This indicates that the electrical properties of these films are also insensitive to current path.

The effect of doping observed in these T_d=325C samples was enhanced relative to that observed in films prepared at lower deposition temperatures (T_d=150C and 250C, see Fig. 4.4). σ(RT) varied by over six orders of magnitude between the undoped and the most heavily doped samples ($2.\times10^{-2}$ B_2H_6/C_2H_2) . This contrasts with the four order of magnitude variation of σ(RT) seen in equivalently doped samples prepared at T_d=250C. As the values of E_A(250) and E_{opt} for the T_d=325C samples are lower than those for the samples prepared at 250C, it may be assumed

that the Fermi level lies closer to the band tails in samples prepared at the higher temperature. Thus, the Fermi level will be more easily driven into the band tail by the same dopant concentration, resulting in the greater increase observed in σ (RT).

The value seen here for $\sigma_o(250)$ in the case of doped samples ranged from 0.15 to 3.9 ohm^{-1}-cm^{-1}. These values are about two orders of magnitude larger than those found for similarly doped samples prepared at T_d=250 or 150C. This result, however, is consistent with the interpretation that the Fermi level in these heavily doped samples lies in a region of relativly high gap state density. Both the mobility and the density of states contribute to σ_o, and both these terms increase as the conduction mechanism moves closer to a mobility edge from within the gap. As both high T_d and heavy doping move the energy at which transport occurs closer to a mobility edge, it is reasonable that large values of σ_o are observed.

Optical absorption studies were performed on several doped thermopower samples, with the result that $E_{opt} \approx 1.5$ eV. This value is also in good agreement with that obtained on earlier undoped samples prepared at T_d=325C. Though the low values obtained for $E_A(250)$ from these samples are indicative of a weakly activated, almost semi-metallic form of conduction(see

later discussion, pg. 103), the persistence of a measurable optical gap indicated that semiconducting properties remained. It is true, however, that the overall behavior(weakly activated conduction, with high values of σ_o) of these films was more "graphitic" in nature than that of previously deposited doped samples. It is therefore likely that in this limit of preparation(T_d=325C, 1.0% dopant), these a-C:H films had a greater tendency towards three-fold coordination than the earlier doped films prepared at T_d=250C. This is consistent with a reduced incorporation of hydrogen at higher T_d.

The magnitude of the thermopower S observed here was in the range $(-60 < S < 60)\mu V/K$, with a typical value of $\sim 30\mu V/K$(See Fig. 4.6). The sign of the observed thermopower was negative for the case of n-type doping(phosphorous), and was positive for the case of p-type doping(boron), thereby verifying a change in majority carrier type upon doping. It is apparent from the magnitude of S that a hopping type transport mechanism must predominate for these samples, as S would take on values roughly two orders of magnitude greater were this conduction via extended states[38].

To analyze the thermopower data obtained here, an analysis similar to that employed by Friedman[22] for thermopower in heavily doped a-Si:H is used. In the

case of hole transport in a-C:H(as the data used in the following analysis was obtained with p-type a-C:H), we assume N(E) in the band tail(with E_b taken as 0) to be of the form of an increasing exponential density of states between E_b and E_v(see Fig. 4.8 for the placement of E_b and E_v),

$$N(E) = N(E_b)\exp[\beta E]$$

thereby allowing the applicability of Eqn. I.7,

$$S(T) = -\frac{\pi^2}{3}(kT)\frac{k}{e}\frac{\partial}{\partial E}\ln(\mu N(E))\Big|_{E=E_F}$$

to be tested. Using the dependence of u(E) on the density of states N(E)[9h], we obtain

$$\mu(E) = \mu[N(E)] = \frac{e\nu_{ph}}{6kT}\left(\frac{9}{8\pi\alpha kTN(E)}\right)^{1/2}\exp\left[-2.1\left(\frac{\alpha^3}{kN(E)}\right)^{1/4}\right]$$

This form of $\mu(E)$ is justified for the case of variable range hopping in energy levels near the Fermi energy. As a validation of the use of this form of the mobility, we not that the conductivity data taken on these heavily doped thermopower samples fit well to the expression appropriate to variable range hopping,

$$\sigma = \sigma_2\exp\left[-\left(\frac{T_o}{T}\right)^{1/4}\right]$$

The values obtained from the data on our most heavily doped sample(A in Fig. 4.6) are $T_o = 1.06\times10^5$K, and

$\sigma_2 = 21.5 \text{ohm}^{-1}\text{-cm}^{-1}$. Using the expressions[12e]

$$T_o = \frac{16\alpha^3}{kN(E_F)} \; ; \quad \sigma_2 = \frac{e^2 N(E_F)(.388)\nu_{ph}}{(\alpha N(E_F)kT)^{1/2}}$$

and taking the values

$$T=500K,\ \alpha^{-1}=20A,\ N(E_F)=5.0\times10^{19}\text{cm}^{-3}\text{-eV}^{-1},\ \nu_{ph}\sim 10^{13}\text{ hz}$$

we calculate $T_o = 4.62\times10^5 K$, and $\sigma_2 = 9.5 \text{ ohm}^{-1}\text{-cm}^{-1}$. Thus, there is reasonably good agreement here between calculated and observed values of these hopping parameters(See pg.106 for a discussion of the values chosen for α^{-1} and $N(E_F)$. The conductivity data for these heavily doped samples also fits well when plotted using the expressions applicable to nearest neighbor hopping, so a definitive separation of these two regimes can not be made here, although the thermopower data definitely indicate that VRH is the actual mechanism.

Replacing N(E) by the assumed exponential form, and taking the logarithmic derivative of the term uN(E), we obtain

$$\frac{\partial}{\partial E} \ln(\mu N(E))\Big|_{E=E_F} = \beta\left\{\frac{1}{2} + \frac{2.1}{4}\left(\frac{\alpha^3}{kT}\right)^{1/4} N(E_F)^{-1/4} \exp\left[-\frac{\beta E_F}{4}\right]\right\} \sim c\beta$$

where c is a weak function of T. The sign of the thermopower in this case is dependent upon the slope of the density of states, which is determined by the sign of β. We note that β is negative in the valence band tail and positive in the conduction band tail.

In order to approximate the above expression as $c\beta$, a simplifying assumption was required. The exponential term appearing in c takes on limiting values between 0 and 1, when the term βE_F varies between 0 and positive infinity. In this case, as energy is measured relative to E_b, and conductivity data indicate that the Fermi level lies in or very near the band tail(based upon large values of σ_o and a weakly activated conductivity), the value of E_F may be taken as being small(~0.02 eV for our most heavily doped sample). An upper bound may be placed upon β by computing how large β would have to be to allow for the rapid rise(2 orders of magnitude in 0.3eV) in gap state density near the mobility edge of amorphous silicon[29]. Since optical absorption and conductivity data indicate a-C:H does not have as low a gap state density as a-Si, setting an upper bound on β in this manner is justified. This yields a value of approximately $\beta=15\ eV^{-1}$, thus $\beta E_F/4=0.075$. It is now evident that approximating the exponential term as unity is a valid assumption.

Using the limiting case of our most heavily doped sample(labeled A in Fig. 4.6), and taking the slope of its plot of S versus $T(1.3\times10^{-7}V/K^2)$, one may compute the result that $c\beta=5.33eV^{-1}$. Therefore, the condition on T such that Eqn. I.7 (Refer to page 24) applies is $T \ll 2200K$, which is the limit in which these measurements were made.

It is possible to calculate the value of c in this case by making several assumptions as to the values of α, T, and $N(E_b)$. Taking approximate values such as $\alpha^{-1}=20A$, $N(E_b)=5.x10^{19}cm^{-3}eV^{-1}$, and T=500K, in the equation above we obtain c=1.25 . The value of α^{-1} chosen here is at the high end of its proposed range[12f]. This was selected as appropriate due to the high gap state density in a-C:H, and the relatively high temperatures at which this work was performed. As localization is relaxed by both of the prior conditions, the use of the large value for α^{-1} seems to be appropriate. The value of $N(E_b)$ was estimated from data on a-Si:H[29]. Next, using the value of $c\beta$ obtained earlier from the slope of S vs. T, we obtain $\beta=4.26eV^{-1}$. Taking our estimated value for the band tail dimension in this case to be $0.6eV(E_v-E_b)$ (obtained in the same manner as for Fig. 4.8), the value of $N(E_v)$ may be estimated by utilizing the assumed exponential form of N(E), and is determined to be

$$N(E_v)=N(E_b)\exp(\beta E)=5.x10^{19}\exp((4.26)(.6))=6.4x10^{20}cm^{-3}ev^{-1}$$

This result is dependent upon the assumed value of $N(E_b)$, as β determines only the ratio between $N(E_v)$ and $N(E_b)$. Thus, the magnitudes of these two quantities as determined above are subject to adjustment, though their ratio is reasonably well

defined.

As a further test of the above analysis, data[29] on a-Si:H from Friedman's paper was used. Reading off a two order of magnitude decrease in gap state density between the conduction band mobility edge(at E_c) and the bottom of the band tail at -0.3eV, a value of approximately β=15 would be required(if the tail state density is modeled as being exponential). Given this, and taking values of α and T used by Nagels[9i] one finds $c\beta$=89.3. Therefore, for a-Si:H, the condition for the validity of Eqn. I.7 becomes $T \ll 130K$. This predicts that any such linear behavior of S with T will only be observed in the limit of very low temperatures for a semiconductor with narrow band tails such as found in a-Si:H.

Beyer and Stuke[39] have observed S to be an increasing function of T in evaporated amorphous silicon and germanium(for $150 < T < 250K$). In their article, the behavior was explained in terms of S being a weighted sum of three components to the thermopower, S_+ (S due to holes), S_- (S due to electrons), and S_H (a constant contribution due to hopping near E_F). It is possible, however, that the regime in which S is an increasing function of T may also be explained in terms of the model proposed here, presuming the condition on Eq. I.7 was met(see page 24). As evaporated films of a-Ge and a-Si have higher

gap state densities than their glow discharge counterparts, it is reasonable to expect that they will have broader band tails, which, according to the thermopower analysis just performed, increases the chances that S will be observed to be a linearly increasing function of T.

Other authors[46,47] have derived expressions predicting that S varies as $T^{1/2}$ in the case of variable range hopping at the Fermi level. The assumption in these cases, however, is that one is dealing with a lightly doped sample, where there exists a donor or acceptor band distinct from the main band structure. In these cases, conduction is thought to take place in these narrow dopant induced bands. As the a-C:H samples that have been studied here are very heavily doped, it is not likely that such a unique band structure would be found. It is noted, however, that the data for S taken here are not inconsistent with a $T^{1/2}$ dependence, as S for these heavily doped samples is a weak function of T measured over a relatively small range of temperatures. Thus, the absolute separation of these two dependences is not be possible given the data at hand.

V) CONCLUSIONS

The undoped semiconducting thin films of hydrogenated amorphous carbon, produced and studied here, have electrical and optical properties which vary quite strongly with deposition temperature T_d. The properties of these films may be summarized as follows:

1) The room temperature electrical conductivity $\sigma(RT)$ varies from 10^{-16} to 10^{-6} ohm^{-1}-cm^{-1}, as T_d is varied from 75 to 350C.
2) The measured conductivity $\sigma(T)$ is neither simply activated, nor is it consistent solely with a variable range hopping mechanism. Instead, activated hopping conduction in a broad range of localized states near one of the band edges is likely, with the additional complication that the dominant conduction processes occur at energies that lie further from E_F as the temperature is raised. This explanation is consistent with the low values of σ_o (10^{-4} to 10^{-2} ohm^{-1}-cm^{-1}) observed, and also with the curvature shown in the $\ln\sigma$ vs $1/T$ plots.

3) The optical gap E_{opt} decreases from 2.1 to 0.9eV as T_d is increased from 25 to 375C, with most of the decrease in E_{opt} occurring for $T_d \geq 250C$.
4) The electrical and optical properties of these a-C:H films appear to extrapolate to those of evaporated or sputtered a-C films, which are primarily "graphitic" in nature, for T_d 425C.

Having established a reliable body of data on undoped a-C:H films, a study of the possibility of doping a-C:H was carried out, the results of which are stated below;

1) Hydrogenated amorphous carbon can be doped. It was shown in the course of this study involving samples prepared at T_d=250C, that E_F could be shifted by a total of 0.7eV through the gap, via the incorporation of boron and phosphorous. Accompanying this shift of E_F was a five order of magnitude variation in σ(RT) (10^{-12} to 10^{-7} ohm^{-1}-cm^{-1}). The verification of successful doping was obtained through electrical conductivity measurements, as well as by thermopower results. This outcome is quite interesting, as the ability to chemically modify a semiconductor's electrical properties is essential if one is to consider the material for

potential device applications. As this is a new result, no device as of yet has been fabricated, but several attempts to do so will be underway shortly.

2) The conduction mechanism of the heavily doped thermopower samples, as indicated by the magnitude of S(10-60uV/K), involves hopping conduction. This process may be modeled self-consistently as taking place near the bottom of the band tails(at E_a or E_b), via the use of the "metallic" thermopower expression(I.7), leading to a linear dependence of S on T.

3) The doping efficiency achieved here is comparable to that found in similarly prepared(via dc glow discharge) hydrogenated amorphous silicon. There is thus the possibility that, upon a switch to rf glow discharge preparation, as is the case with silicon, a two order of magnitude increase in doping efficiency may be observed.

There still is a considerable amount of work that could be performed to better characterize this new and rather interesting material. The first line of work I believe should be pursued would be the characterization of both doped and undoped films of hydrogenated amorphous carbon prepared via rf discharge techniques. Though work has been done on undoped rf films, it would be of considerable interest to determine what the effect

a switch to a rf discharge would have upon both the doping efficiency, and the conduction mechanism at work. One major difficulty in the way of device fabrication of this material is the large width of the band tails. Perhaps when one utilizes rf techniques, the hydrogen may bond into the material more effectively(in such a manner as to more completely remove states from the gap), thus reducing the gap states density, as well as narrowing the band tails. As a reduced gap state density is closely linked to improved doping sensitivity, this line of research seems promising.

It would be profitable to resolve the question of what fraction of the carbon atoms in a-C:H are three or four-fold coordinated, and to establish the relationship between this and the optical and electrical properties observed. There is some dispute at present as to whether there are four-fold coordinated carbon atoms in amorphous carbon[48,49], but generally the material has been prepared without the incorporation of hydrogen, either by ion beam or evaporative deposition techniques. A study of the relationship between hydrogen incorporation and the coordination number of the carbon atoms would help to resolve this question.

From the point of view of this material's physical properties, it would be interesting to test the

dimensions to which films of this material may be produced. As these films are exceptionally hard and chemically inert, the preparation of thick films of this material would open the way for a great number of applications where such properties are desirable(ie. surface coating for devices subject to erosion, either chemical or mechanical).

In conclusion, this is quite an interesting new material, and though it will have only limited use in its current form, the doors for further improvement and additional work are wide open, and it is quite conceivable that a good deal of advance may yet be made in the further modification and study of hydrogenated amorphous carbon.

REFERENCES

1) Proceeding of the Eighth International Conference on Amorphous and Liquid Semiconductors, Ed. W. Paul and M. Kastner, North Holland Publishing, Amsterdam, 1a)text, 1b)pg.707ff, (1980).

2) W. Spear and P. LeComber, Solid State Comm. 17, 9(1975).

3) A. Mearns, Thin Solid Films 3, 201(1969).

4) L. Holland and S. Ojha, Thin Solid Films 38, 217(1976).

5) B. Carbajal, Transactions of the Metallurgical Society of AIME, 236, 364(1966).

6) D. Anderson, Phil. Mag. 35, 17(1977).

7) D. Weaire and M. Thorpe, Phys. Rev. B4, 2508(1971).

8) M. Thorpe and D. Weaire, Phys. Rev. B4, 3518(1971).

9) Topics in Applied Physics, 36, Amorphous Semiconductors. Edited by M. Brodsky, Springer Verlag(1979), 9a)pg.21, 9b)pg.252, 9c)pg.124 9d)pg.141, 9e)pg.142, 9f)pg.253 9g)pg.123 9h)pg.143 9i)pg.127 9j)pg.80.

10) P. Viktorovitch and D. Jousse, J. of Non-Crystalline Solids 35 & 36, 569(1980).

11) J. Cohen et al., J. of Non-Crystalline Solids 35 & 36 , 581(1980).

12) Electronic Processes in Non-Crystalline Solids (2nd Ed.), N. Mott and E. Davis, Clarendon Press, Oxford(1979), 12a)pg.210, 12b)pg.15, 12c)pg.366, 12d)pg.54, 12e)pg.34, 12f)pg.358.

13) P. LeComber and W. Spear, Phys. Rev. Lett. 25 509(1970).

14) D. Thouless, Phys. Rev. C 13, 93(1974).

15) R. Kubo, Can. J. Phys. 34, 1274(1956).

16) D. Greenwood, Proc. Phys. Soc.(London) 71, 585(1958).

17) N. Mott, Phil. Mag. 22, 7(1970).

18) N. Mott, Phil. Mag. 19, 835(1968).

19) T. Holstein, Ann. Phys. (N.Y.)8, 343(1959).

20) G. A. Connel, D. Camphausen, and W. Paul, Phil. Mag. 26 541(1972).

21) M. Cutler and N. Mott, Phys. Rev. 181, 1336(1969).

22) L. Friedman, Phil. Mag. 36 553(1977).

23) M. Brodsky, M. Cardona, and J. Cuomo, Phys Rev B16, 3556(1977).

24) S. Ojha, and L. Holland, Proc. Seventh Intern. Vac. Congr. & Third Intern. Conf. on Sol. Surf., Vienna 1667(1977).

25) F. Vastola and J Wightman, J Appl. Chem. 14, 69(1964).

26) S. Ojha, N. Narstrom, and D McCulluch, Thin Solid Films 60, 213(1979).

27) J. Tauc, Optical Properties of Solids, Edited by F. Abeles, North Holland(1969).

28) E. Davis and N. Mott, Phil. Mag 22, 903(1970).

29) W. Spear and P. LeComber, Phil. Mag. 33, 935(1976).

30) W. Braker and A. Mossman, Matheson Gas Data Book(Fifth Ed.) Matheson 1971.

31) W. Braker, A. Mossman, and D. Seigel, Effects of Exposure to Toxic Gases, First Aid and Medical Treatment(2nd Ed.) Matheson 1977.

32) D. Whitmell and R. Williamson, Thin Solid Films 35 255(1976).

33) D. Carlson, C. Wronski, A. Triano, and A. Daniel, 12th IEEE Photovoltaics Specialists Conf., IEEE, N.Y. 93(1976).

34) D. Carlson, C Wronski, J. Electronics Materials 6 95(1977).

35) M. Ozaki, D. Peebles, B. Weinberger, C. Chiang, S. Gau, A. Heeger, and A. MacDiarmid, Appl. Phys. Lett. 35 83(1979).

36) Keithly Electrometer Measurements, Revised 2nd Ed., Cleveland, Ohio, 1977.

37) H. M. Kizilyalli and P. R. Mason, Phys. Stat. Sol. A 36 499(1976).

38) D. Jones, P. LeComber, and W. Spear, Phil. Mag. 36 54(1977).

39) W. Beyer, and J. Stuke, Fifth Int. Conf. on Amorphous and Liquid Semi. Ed. J. Stuke and W. Brenig, Taylor and Francis, London 251(1974).

40) R. Gambino, and J. Thompson, Solid State Com. 34 15(1979).

41) S. Oguz, R. Calline, M. Paesler, and W. Paul, J. Non-Crys. Solids 35 & 36, 231(1980).

42) J. Hauser, J. Non-Crys. Solids 23, 21(1977).

43) J. Lannin, Proc. Seventh Int. Conf. on Amorphous and Liquid Semi. Ed. W. Spear, Univ. of Edinburgh, 110(1977).

44) B. Roedern, L. Ley, M. Cardona, and F. W. Smith, Phil. Mag. B40, 433(1979).

45) B. Scott, and M. Brodsky, private communication

46) H. Overhof, Phys. Stat. Sol. B67, 709(1975).

47) V. Zvyagin, Phys Stat. Sol. B58 443(1973).

48) N. Wada, P. Gaczi, and S. Solin, J. Non-Crystalline Solids 35&36, 543(1980)

49) S. Solin, N. Wada, and J. Wong, Proc. of the 14th Int. Conf. on the Phys. of Semi., Ed. B. Wilson, The Institute of Physics Bristol and London, 721(1978)